NSWC TR 88-362

MICROWAVE INTERFEROMETRIC MEASUREMENTS OF PARTICLE AND WAVE VELOCITIES IN POROUS MEDIA

BY BRIAN C. GLANCY (NSWC)
ALBERT D. KRALL (ATR)

RESEARCH AND TECHNOLOGY DEPARTMENT

11 JANUARY 1990

NAVAL SURFACE WARFARE CENTER

Dahlgren, Virginia 22448-5000 • Silver Spring, Maryland 20903-5000

UNCLASSIFIED

SECURITY CLASSIFICATION OF THIS PAGE

REPORT DOCUMENTATION PAGE

1a REPORT SECURITY CLASSIFICATION UNCLASSIFIED	1b RESTRICTIVE MARKINGS
2a SECURITY CLASSIFICATION AUTHORITY	3 DISTRIBUTION / AVAILABILITY OF REPORT Approved for public release: distribution is unlimited
2b DECLASSIFICATION / DOWNGRADING SCHEDULE	
4 PERFORMING ORGANIZATION REPORT NUMBER(S) NSWC TR 88-362	5 MONITORING ORGANIZATION REPORT NUMBER(S)
6a NAME OF PERFORMING ORGANIZATION Naval Surface Warfare Center (NSWC) 6b OFFICE SYMBOL (If applicable) R13	7a NAME OF MONITORING ORGANIZATION
6c ADDRESS (City, State, and ZIP Code) 10901 New Hampshire Ave. Silver Spring, MD 20903-5000	7b ADDRESS (City, State, and ZIP Code)
8a NAME OF FUNDING / SPONSORING ORGANIZATION NSWC and SSP 8b OFFICE SYMBOL (If applicable)	9 PROCUREMENT INSTRUMENT IDENTIFICATION NUMBER
8c ADDRESS (City, State, and ZIP Code) Strategic Systems Programs (SSP) Washington, DC 20376	10 SOURCE OF FUNDING NUMBERS PROGRAM ELEMENT NO: 64363N, 61152 / PROJECT NO: J0951, 7R00001 / TASK NO: J0951, 7R013 / WORK UNIT ACCESSION NO: R23DF, R01AC262

11 TITLE (Include Security Classification)
Microwave Interferometric Measurements of Particle and Wave Velocities in Porous Media

12 PERSONAL AUTHOR(S)
Glancy, Brian C. (NSWC) and Krall, Albert D. (ATR)

13a TYPE OF REPORT	13b TIME COVERED	14 DATE OF REPORT (Year, Month, Day)	15 PAGE COUNT
Progress	FROM 01-84 TO 06-88	1990, January, 11	82

16 SUPPLEMENTARY NOTATION

17 COSATI CODES		
FIELD	GROUP	SUB-GROUP
21	08	02
19	01	

18 SUBJECT TERMS (Continue on reverse if necessary and identify by block number)
Microwave Interfermetry, Wave Front Motion, Beat Fringe Analysis, Impedance Matching, Detonation Physics, Dielectric Measurements

19 ABSTRACT (Continue on reverse if necessary and identify by block number)

A microwave interferometric technique was developed and integrated with several experimental arrangements for detonation physics studies. The interferometer records the Doppler shift of reflections associated with moving material discontinuities and ionization fronts. The analysis of those Doppler shifts provide quantitative velocities which are useful in the development and verification of physical and theoretical models used to depict the processes. Initial circuit criteria such as impedance matching, dielectric measurements, and waveguide modes are considered. The interferometer has been applied to detonation velocity measurements, detonation transfer tests, gap testing, and piston driven compaction experiments. In addition to the relatively simple analysis used to obtain these results, investigations into higher resolution data reduction aided by computer synthesis and Fourier transforms are also discussed.

20 DISTRIBUTION / AVAILABILITY OF ABSTRACT	21 ABSTRACT SECURITY CLASSIFICATION
☒ UNCLASSIFIED/UNLIMITED ☐ SAME AS RPT ☐ DTIC USERS	UNCLASSIFIED
22a NAME OF RESPONSIBLE INDIVIDUAL Brian C. Glancy	22b TELEPHONE (Include Area Code) 202/394-1096 / 22c OFFICE SYMBOL R13

DD FORM 1473, 84 MAR — 83 APR edition may be used until exhausted. All other editions are obsolete.

SECURITY CLASSIFICATION OF THIS PAGE
UNCLASSIFIED

GPO: Government Printing Office 1988—630-812

FOREWORD

A microwave interferometer has been developed and integrated with ongoing shock-to-detonation and deflagration-to-detonation transition experiments on porous energetic materials. Microwave interferometry is a continuous, non-intrusive technique which is especially well suited to high confinement tests where optical and x-ray techniques can no longer be easily used to observe the events. Most energetic materials, even aluminized ones, readly transmit microwave power, while partially or fully reflecting that power at locations of chemical reaction or compressive/shock waves. In addition to locating both reactive and non-reactive fronts, the relative absorption and reflection of microwaves is expected to provide information about the dynamic processes. This report discusses the technique, the NSWC interferometric circuit and its tuning, and the application of this instrumentation in several types of experiments. Both the data from those experiments and the various methods used to analyze output data are discussed. This work was accomplished for the NSWC Independent Research program and the Hazard Assessments of Rocket Propellants (HARP) program.

The authors wish to express their gratitude to Dr. R. Bernecker and Dr. H. Sandusky for guidance and support received during the course of the work. They are indebted to Dr. S. Jacobs for his critical review of this manuscript. Also, the assistance of C. Groves and P. Femiano was greatly appreciated for the proper execution of the experiments.

Approved by:

William H. Bohli

WILLIAM H. BOHLI, Head
Energetic Materials Division

CONTENTS

Chapter		Page
1	INTRODUCTION	1-1
2	MICROWAVE INTERFEROMETER	2-1
	INTERFEROMETRIC CIRCUIT	2-1
	CIRCUIT TUNING	2-6
	IMPEDANCE MATCHING OF INTERFEROMETER WITH TEST SAMPLE	2-7
	CIRCULAR WAVEGUIDE	2-9
3	DIELECTRIC MEASUREMENTS	3-1
	INTRODUCTION	3-1
	AUTOMATED DIELECTRIC MEASUREMENT SYSTEM	3-2
	CAVITY RESONANCE METHOD	3-4
4	INTERFEROMETRIC SIGNAL ANALYSIS	4-1
5	INTERFEROMETRIC MEASUREMENTS FROM VARIOUS ARRANGEMENTS	5-1
	SIMPLE DETONATION VELOCITY AND DETONATION TRANSFER EXPERIMENTS	5-1
	SHOCK WAVE REFLECTIONS	5-8
	GAP TYPE EXPERIMENTS	5-10
	PISTON DRIVEN COMPACTION APPARATUS TESTING	5-20
6	COMPUTER ANALYSIS TECHNIQUES	6-1
	WAVEFORM SYNTHESIS	6-1
	FAST FOURIER TRANSFORM ANALYSIS	6-1
7	CONCLUSIONS AND SUMMARY	7-1
	REFERENCES	8-1
	DISTRIBUTION	(1)

ILLUSTRATIONS

Figure		Page
2-1	SCHEMATIC OF NSWC INTERFEROMETRIC CIRCUIT	2-2
2-2	IDEAL, CONSTANT VELOCITY REFLECTOR, QUADRATURE SIGNAL	2-4
2-3	CIRCULAR WAVEGUIDE ALIGNMENT FLANGE SETUP WITH ALIGNMENT PINS SHOWN	2-11
3-1	VARIATION OF DIELECTRIC CONSTANT WITH DENSITY FOR CLASS D HMX AT 8.3 GHz	3-3
3-2	VARIATION OF DIELECTRIC CONSTANT WITH FREQUENCY AT 25°C (ALSO SINGLE FREQUENCY MEASUREMENTS (*) OF ENERGETIC MATERIALS)	3-6
3-3	VARIATION OF DIELECTRIC CONSTANT WITH DENSITY FOR MIXTURES OF MELAMINE AND ALUMINUM AT 8.3 GHz	3-7
4-1	MODEL OF MICROWAVE REFLECTION FROM A SHOCK FRONT	4-2
4-2	RAW DATA FROM PISTON IMPACT EXPERIMENT SHOWING SUPERIMPOSED FRINGES	4-5
4-3	MODEL FOR PISTON AND COMPRESSIVE WAVE REFLECTIONS	4-6
5-1	RECTANGULAR WAVEGUIDE SETUP WITH TEFLON WEDGE AS MATCHING SECTION	5-2
5-2	OUTPUT FRINGES FROM RP-80 INITIATED DETONATION OF 73.0% TMD CLASS D HMX WITHIN RECTANGULAR WAVEGUIDE	5-3
5-3	DISPLACEMENT VERSUS TIME FOR RP-80 INITIATION OF DETONATION IN CLASS D HMX IN RECTANGULAR WAVEGUIDE	5-5

ILLUSTRATIONS (Cont.)

Figure Page

5-4 OUTPUT FRINGES FROM DETONATION TRANSFER TEST ,M-7, USING COMPOSITE BED OF HMX/NaCl/HMX 5-6

5-5 DISPLACEMENT-TIME HISTORY COMPARISON OF TWO HMX/NaCl/HMX DETONATION TRANSFER TESTS 5-7

5-6 OUTPUT FRINGES SHOWING DC SHIFT FROM HMX EXPLOSIVE SHOCKING TEFLON 7C 5-9

5-7 TEST SECTION SHOWING USE OF 1/4 WAVE MATCHING PLUG, FOR CLASS D HMX EXPLOSIVE SHOCKING ALUMINIZED INERT . . . 5-11

5-8 OUTPUT FRINGES FROM CLASS D HMX EXPLOSIVE SHOCKING 30% ALUMINIZED MELAMINE IN CIRCULAR WAVEGUIDE 5-12

5-9 DISPLACEMENT-TIME HISTORY OF EXPLOSIVE SHOCKING 30% ALUMINIZED MELAMINE DATA IN CIRCULAR WAVEGUIDE . 5-13

5-10 SETUP FOR A GAP EXPERIMENT, INTERFACED WITH MICROWAVE INTERFEROMETER 5-14

5-11 RAW DATA FROM TYPE "A" FLUID BALL POWDER GAP TEST . . . 5-15

5-12 COMPARISON OF CAMERA RECORD WITH INTERFEROMETRIC DATA FOR GAP EXPERIMENT OF FIGURE 5-10 5-17

5-13 RAW DATA FOR 65% TMD CLASS D HMX GAP EXPERIMENT, IMPEDANCE MATCHED 5-19

5-14 PDC APPARATUS INTERFACED WITH MICROWAVE INTERFEROMETER 5-21

5-15 INITIAL REDUCTION OF SUPERIMPOSED DATA SHOWING DISAGREEMENT OF PISTON FRONT MOTION 5-22

5-16 REVISED REDUCTION OF SUPERIMPOSED FRINGES USING EQUATION (4-5) SHOWING BETTER AGREEMENT 5-24

ILLUSTRATIONS (Cont.)

Figure		Page
6-1	ANALYTICAL MODEL FOR HIGHER HARMONICS	6-4
6-2	DIELECTRICS REQUIRED TO MAXIMIZE PARTICULAR HARMONICS .	6-6
6-3	MELAMINE RAW DATA FRINGES WITH MISMATCHED INTERFACE . .	6-8
6-4	FREQUENCY DOMAIN DATA FROM MISMATCHED MELAMINE TEST . .	6-9
6-5	MISMATCHED MELAMINE DATA FILTERED TO REVEAL THE FUNDAMENTAL PISTON REFLECTION	6-11

TABLES

Table		Page
6-1	VALUE OF TRANSMISSION COEFFICIENT NEEDED TO MAXIMIZE ANY PARTICULAR DOPPLER HARMONIC	6-5

CHAPTER 1

INTRODUCTION

Microwave interferometry is a non-perturbing technique, suitable for continuously monitoring the propagation of reaction fronts in energetic materials or compressive waves and shock fronts in any material. The fact that microwaves penetrate most energetic materials with very little loss and negligible effect makes this method feasible. Equally important is the fact that microwaves are at least partially reflected by shock waves and reaction fronts. Thus, microwaves can "*look into*" materials continuously and non-intrusively while monitoring the location of moving reflection zones. The results of these investigations provide quantitative data for the improvement or verification of models being developed to predict the shock-to-detonation transition (SDT) and the deflagration-to-detonation transition (DDT).

Much of the current understanding of SDT has been obtained by high-speed photography of unconfined solid charges or weakly confined porous charges. High-speed photography and flash radiography of weakly confined porous charges have been essential in elucidating the DDT mechanism. Modeling these experiments is complicated by the loss of confinement, especially when the event is not prompt, as in DDT. Therefore, more highly confined experiments, often using thick wall steel tubes, are desired to support "*one-dimensional*" modeling efforts. The drawback is that these tubes are not suitable for high-speed photography and flash radiography. The experiments still need to be well instrumented, but the available methods primarily involve inserting ionization probes and pressure transducers through the wall of the tube. The disadvantages of probes and transducers include weakening the confinement, being only discreetly located, and affecting the event if they are not flush with the inner wall. Microwaves, on the other hand, can be transmitted into the downstream end of confined material to provide a continuous record of front positions without any of the aforementioned disadvantages.

Early studies of energetic material detonation velocities using microwave interferometry began in Germany during World War II by Lochte-Holtgreven and Koch. The first available report of this work was given by Koch[1] in 1953. The experiments resembled the operation of radar in that a microwave signal at 1.3 GHz was transmitted and received through air, via an antenna. The signal from the antenna traveled to the unconfined explosive and a small fraction of it was reflected from the detonation front. Since the front was moving, a Doppler shift was added to the reflected wave and when received, allowed processing to determine the frontal velocity. These experiments were repeated at 9.4 GHz on different materials in the United States by Cook, Doran and Morris[2] in 1955. The problem with these open experiments is that the wavelength in the explosive was unknown and thus the velocity could only be estimated.

A little later, Cawsey, Farrands, and Thomas[3] in Australia used an interferometer that totally encased the explosive in a 35 GHz metallic, rectangular waveguide. This modification allowed an exact knowledge of the electromagnetic waves (wavelengths) within the sample. In the mid 1960's, Johnson[4] at Redstone Arsenal used an interferometer to couple the signal directly into an unconfined energetic material that served as a dielectric rod to observe the growth-to-detonation using a microwave interferometer compared with streak camera results. Here, the sample was again unconfined, but the knowledge of unconfined electromagnetic waves was well defined by this time. In 1973, Alkidas, Clary, Giles, and Shelton[5] at the Georgia Institute of Technology developed an interferometer that measured the phase change from the reflected signal of a burning propellant. This system differs from most interferometers which measure the rate of change of phase (Doppler frequency). The arrangement enabled them to increase their resolution from 180 degrees (one-half cycle) to 0.2 degrees. Russell[6] pressurized his burning propellants and used an interferometer to determine the burning rates at elevated pressures. By 1986, microwave techniques had matured to the point where Stanton, Venturini, and Dietzel[7] reported on the development of three interferometers at 10, 35, and 91 GHz. They emphasized tuning, signal canceling, quadrature detection, and monitoring of the return signal intensity, all in an effort to obtain precise and accurate data in studies of SDT and DDT.

At Naval Surface Warfare Center (NSWC), an x-band (8.2 to 12.4 GHz) microwave displacement interferometer has been developed. The interferometric circuit is based on that used by Stanton, et al.,[7] at the Sandia National Laboratories. In this interferometer, a single frequency source signal is split into two portions, a reference signal and a test signal. The test signal is guided to, and enters, the downstream end of the test sample which is enclosed in conductive waveguide. Microwave reflections occur at ionized reaction zones or dielectric discontinuities. A portion of the incident microwave signal is reflected at the discontinuity caused by the leading compressive front. Any remaining signal passes through the front to be reflected from other moving discontinuities in the experimental sample. Since the reflectors of interest move, a Doppler shift in frequency is added to the microwave frequency. The Doppler shifted return signal is received by the detector (mixer) where it combines with the reference signal to produce a Doppler frequency "*beat fringe*" output--video frequency signals (DC to 10 MHz) defined by the difference between the reference and the reflected test signals. The output of the interferometric mixer can be analyzed to give displacement versus time histories of the various reflection fronts.

A major problem in the interpretation of the recorded waveforms is distortion. Development of an automated dielectric constant measurement system[8] at NSWC has allowed the application of improved matching techniques to remove some of the unwanted reflections that cause distortion. This is accomplished by impedance matching[9] between the dielectric constant of the air which fills the empty waveguide and that of the higher dielectric of the test bed, also confined in the waveguide. Unwanted reflections cause distortion in the output fringes by developing harmonics and by exciting higher order modes. These signals, superimposed on the desired reflections, form the resultant waveform and introduce additional obstacles to overcome in the analysis of resulting data. Even with perfectly matched equipment and materials, there is still a residual output distortion that is intrinsically produced by the mechanism being investigated. Signal processing must then be used to decipher the output and separate it into its precisely measurable components. Synthesis of signals was first tried and was helpful for the simplest of distortions. Currently, development of Fourier transform analysis methods for more complicated signals is being attempted.

The interferometric technique has been applied to investigate SDT and the latter stages of DDT in porous energetic materials. Information and discussions on the development of this technique cover simple SDT testing in both rectangular and circular waveguide experiments, and interfaces developed for use with two-dimensional shock initiation (gap) experiments and the piston driven compaction (PDC) apparatus. Most of the work reported here has been performed in conjunction with more conventional diagnostic techniques in order to verify the results. Along with the evolution of the interferometric technique, analytic models were required to understand the reduction of test data. These analytic models are presented for clarity. Much of the data analysis results from a straight forward measurement of a single reflecting front, but the more complex analysis of multiple reflections is also presented. The successful application of Fourier transform methods in separating the constituent reflected waveforms is expected to improved the resolution of reduced data. This methodology is being pursued and preliminary data are presented.

CHAPTER 2

MICROWAVE INTERFEROMETER

Interferometric Circuit

The interferometric circuit (shown schematically in Figure 2-1) is suitable for use with any microwave frequency. In practice, an x-band (8.2 to 12.4 GHz) circuit is used since many components are readily available in this frequency range. The circuit is put together with rectangular waveguide of dimensions 0.400 x 0.900 in (10.16 x 22.86 mm) because rectangular waveguide has lower losses compared to coaxial cabling.

As shown in Figure 2-1, the source signal is routed through an isolator and a manual waveguide switch to the first passive device, a 20 dB coupler, where 1/100 of the signal is split off to be used later for tuning. The major portion of the source signal is guided to a 10 dB directional coupler, where approximately one tenth of the signal is removed for use as a reference signal in the quadrature mixer. The remaining signal which passes through the coupler is used as the test signal and is guided through a directional isolator, a reversed 3 dB directional coupler, a second switch, a sliding stub tuner, and an electric isolator before being directed to the test section. The electric isolator prevents any electrical energy from being transmitted, by the conductive portion of the guide, to or from the energetic material. Beyond this isolator there are 2 to 4 m of waveguide passing through the firing chamber wall to reach the test section some distance within. The test section consists of an experimental apparatus that serves as the waveguide which is loaded with the material being tested. Originally, a section of x-band rectangular waveguide was used for technique development; later, a transition section, opening to 25.4 mm inner diameter (ID) circular waveguide, was developed to integrate with ongoing testing.

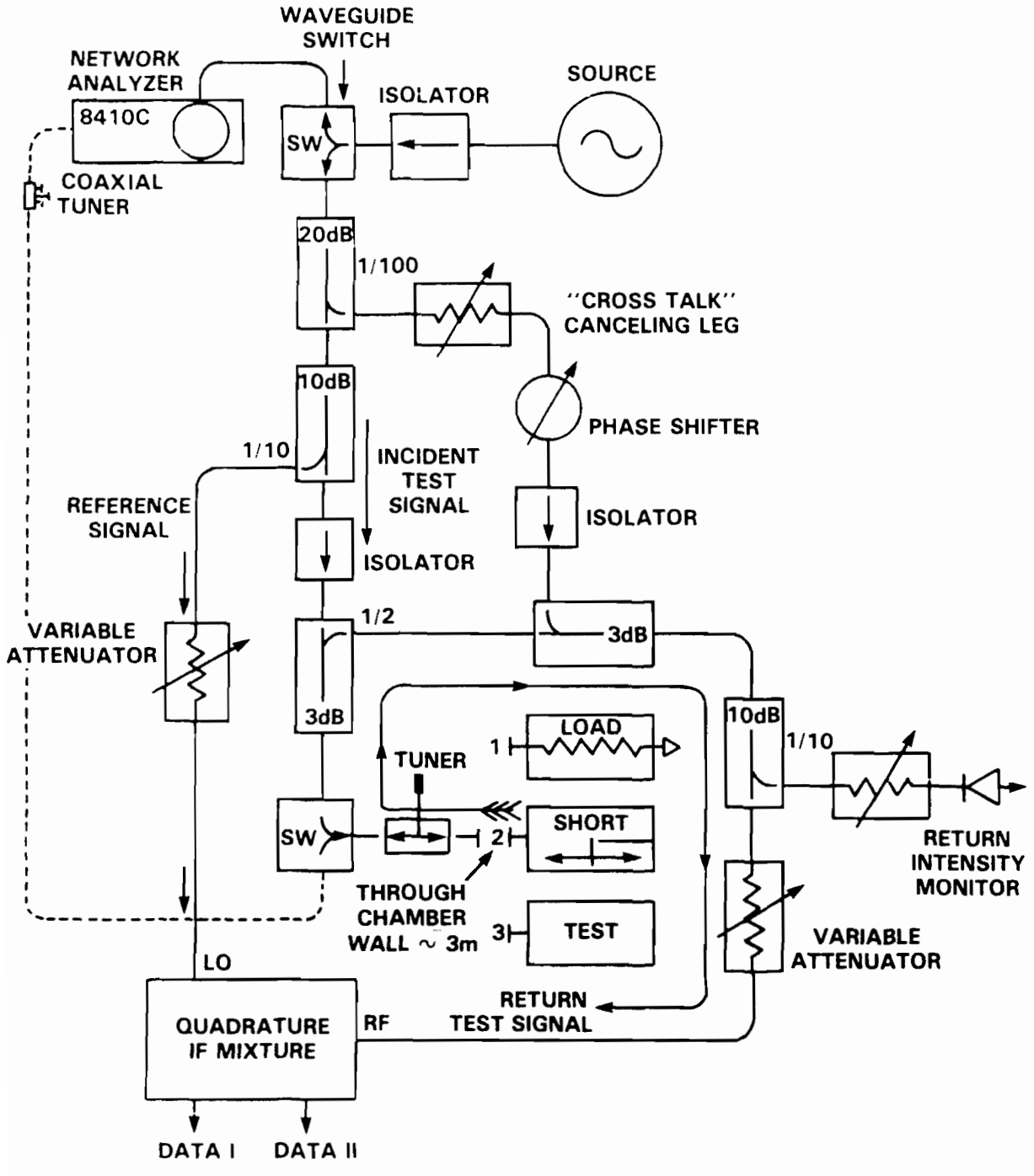

FIGURE 2-1 SCHEMATIC OF NSWC INTERFEROMETRIC CIRCUIT

When the incident microwave signal is reflected from discontinuities within the test, the signal travels back along the same path until encountering the reversed 3 dB coupler. At that point, the reflected test signal is directed to flow only out of the split leg of the coupler due to the action of the directional isolator. The signal then follows along the rest of the interferometer's test leg where it is combined with the signal split from the source by the 20 dB coupler. This small signal is phase shifted and amplitude adjusted to cancel the "*cross-talk*" occurring due to the limited directivity of the reversed 3 dB directional coupler. (In other interferometers,[7] a circulator is used in place of the reversed 3 dB coupler and isolator, yet cross-talk in circulators still requires a small cancellation signal.) The "*corrected*" return signal is then guided into the quadrature mixer after 1/10 of the signal is split off as a reflected intensity monitor. In the mixer, the reference and return signals are combined to form a Doppler shifted output "*beat*" fringe, which is further split to form a quadrature record (2 signals separated in phase by $\frac{\pi}{2}$, or 90 degrees) to increase the accuracy of analysis techniques.

In analyzing an output beat signal, the portion of the fringe which changes at the highest rate gives data having the best resolution. To improve continuous resolution, the fringe signal is repeated such that when one signal is reaching a peak in its output (poorest resolution), the other is sweeping through its greatest change in slope. An example of mixer output from an "*ideal*" total reflector moving at constant velocity within a test is given in Figure 2-2. It shows two perfect sine waves in quadrature (separated by $\frac{\pi}{2}$ in phase). It is the quadrature signal that is analyzed to reveal the displacement histories of the moving reflectors within the walls of the confined test sample. The instantaneous amplitude of these two signals from the quadrature detector can be written as

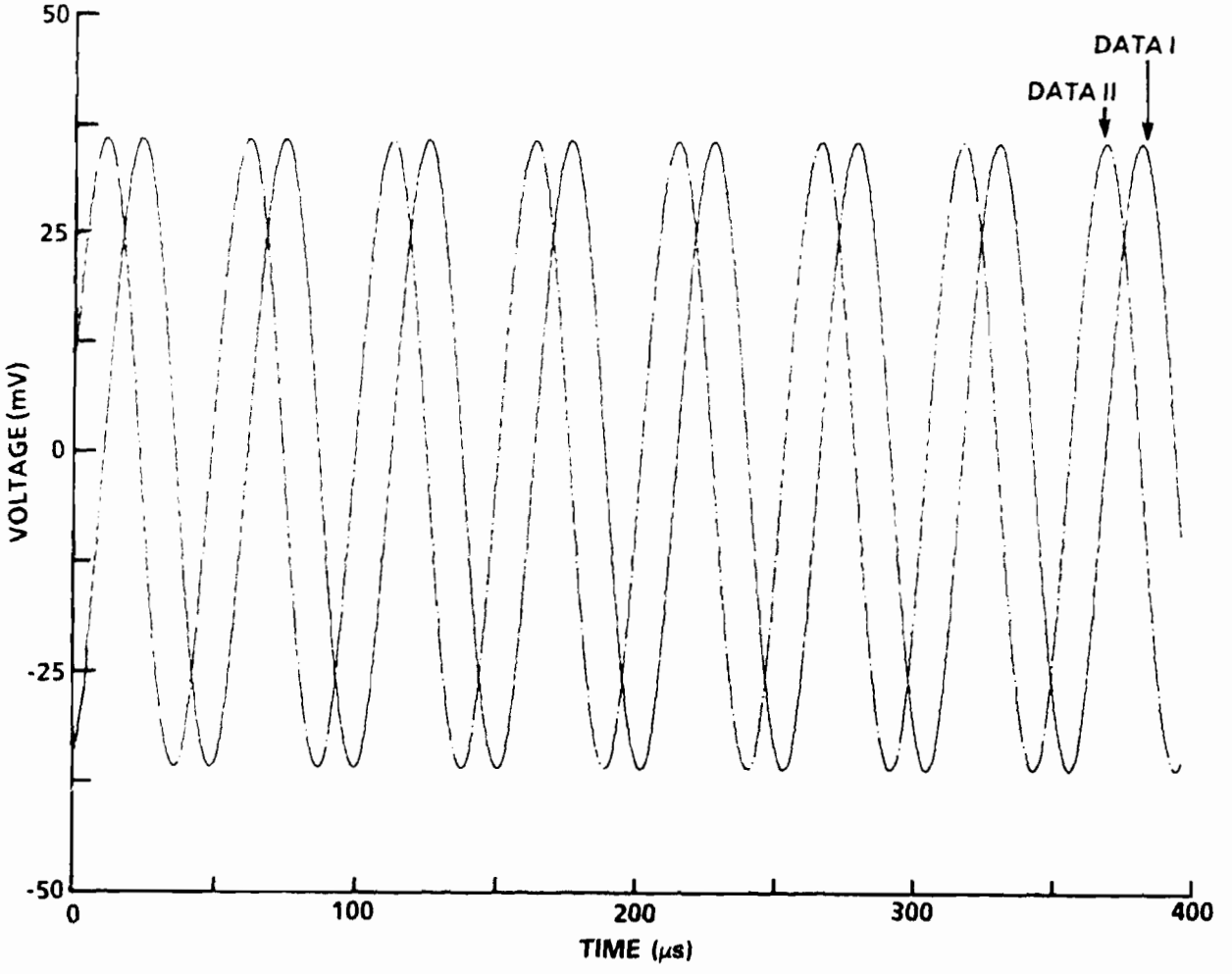

FIGURE 2-2. IDEAL, CONSTANT VELOCITY REFLECTOR, QUADRATURE SIGNAL

$$\text{Data I} = f(x)e^{2\alpha x} \cos 2\beta x(t), \text{ and} \tag{2-1}$$

$$\text{Data II} = f(x)e^{2\alpha x} \sin 2\beta x(t), \tag{2-2}$$

where

$x(t)$ = distance from the reflecting surface at time t

α = attenuation constant

β = phase constant = $2\pi/\lambda_g$

λ_g = waveguide wavelength in the dielectric sample

$e^{2\alpha x}$ = round trip absorption loss in the sample

$f(x)$ = conversion function of matched detectors.[9]

Dividing Equation (2-1) into Equation (2-2) produces

$$\frac{\text{Data II}}{\text{Data I}} = \frac{f(x)e^{2\alpha x}}{f(x)e^{2\alpha x}} * \frac{\sin 2\beta x(t)}{\cos 2\beta x(t)} = \tan 2\beta x(t), \tag{2-3}$$

and by taking the inverse tangent and solving for position,

$$x(t) = \lambda_g * \{ \tan^{-1} [\text{Data II} / \text{Data I}] \}/4\pi \ . \tag{2-4}$$

In order for the position of the reflector in Equation (2-4) to move continuously with time, the discontinuous arctangent function must be incremented by π at each asymptote.

Ignoring other considerations, it can be seen from Equation (2-4) that the interferometer should operate at the highest possible frequency, to provide the highest resolution. However, if the waveguide size is fixed and the frequency is increased without limit, other higher order mode patterns will be excited in addition to the dominant mode. Each of these higher order modes have different velocities. They not only arrive at the detector at different times but also have different field patterns which will not always be detected. The result is distorted sinusoidal output from the interferometric circuit. If, on the other hand, the waveguide size is reduced as the frequency is increased to allow only the dominant mode to propagate, the critical diameter[8] of the energetic materials would be reached. Compromise within these constraints must be and have been made.

One major consideration in this work was the need to integrate the testing circuit with ongoing SDT/DDT experimental studies. Some of the studies are performed in 25.4 mm (1 in) ID cylinders. Fortunately, it is a simple matter to convert from the dominant transverse electric mode, TE_{01}, of a rectangular waveguide to the dominant TE_{11} mode of a circular waveguide using a commercially available tapered section. To avoid exciting higher order modes in the 25.4 mm ID circular waveguide, it is necessary to restrict the upper operating frequency to 9 GHz. These compromises resulted in the use of an interferometric circuit with an x-band source signal ranging between 8.2 and 9.0 GHz in predominantly rectangular waveguide, which is usually transformed to circular waveguide for the energetic samples.

Circuit Tuning

Proper tuning of the circuit is necessary to record accurate information with the interferometer. A mistuned circuit can result in the reflection of part of the return signal which appears as harmonic distorion to the output. The distortions produce an uncertainty in determining the Doppler frequency. Initial circuit tuning is accomplished by careful adjustment of passive waveguide components while monitoring changes with a network analyzer (NA). The NA is a commercial instrument that permits the impedance of a microwave circuit to be determined. Two waveguide switches in the interferometric circuit (SW in Figure 2-1) are used to bypass the main portion of the circuit and allow the source signal to be routed through a NA to tune only the test leg of the circuit which is beyond the second switch. A matched waveguide load is mounted to the second waveguide switch in place of the sliding stub tuner which is located at its output (just outside the chamber wall in Figure 2-1). The coaxial tuner, located at the output switch jack of the NA, is then adjusted until the NA shows zero reflection, thus tuning out any mismatches or reflections between the NA and the second switch. The load is removed and the test leg is reconnected to the circuit with the load now mounted at the end of the leg in place of the test sample. Next, the sliding stub tuner just beyond the second switch is adjusted to null-out any unwanted reflections detected by the NA in this last part of the line. The use of the NA is complete at this point, and the switches are set to route the source signal through the interferometric circuit.

To complete the tuning, the matched load is replaced with a motorized sliding short. This apparatus drives a microwave short (total reflector) periodically back and forth within a section of

waveguide. The moving short adds the Doppler component to the microwave reflection which is needed to produce an output from the quadrature detector. The directivity bleed-through of the reversed 3dB coupler is unwanted and can be canceled while the sliding short is reciprocating. This is accomplished by adjusting the phase shifter and attenuator combination to reduce reflected intensity variations while the sliding short is operating. Also, any other unwanted reflections that were not previously canceled get tuned out in this process. Next, the outputs from the quadrature mixer are displayed on an oscilloscope in x-y mode. Constant motion of the motorized short yields output from the mixer of two quadrature displaced sine waves. Ideally, their combined Lissajous pattern in x-y space forms a perfect circle. The pattern is adjusted to obtain the best approximation to a circle using the attenuators on the input legs of the mixer as a final tuning step. These adjustments are necessary to maintain the detector inputs below their saturation levels. At this point the circuit is considered tuned, and the test section is mounted in place of the sliding short.

Impedance Matching of Interferometer with Test Sample

Dielectric discontinuities within the experimental section produce additional reflections which distort the recorded data. Microwave impedance matching techniques[9] should be used to reduce these distortions to obtain high resolution data from manual reduction of the fundamental output waveforms. The easiest way to reduce dielectric discontinuities is to adjust the various material densities, using a technique to be discussed later, until all materials have identical dielectric constants. Since this is not always practical because of experimental constraints or the termination of a sample to air, a simple quarter-wave dielectric matching section can be inserted as required. Each experiment is performed at a single, known frequency which permits these narrow band matching techniques to be effective. Constructing an impedance matching section begins with calculating the wavelength of the microwave frequency in a waveguide filled with the dielectric test material, and the impedance (Z) of the waveguide. The guide wavelength (λ_g) inside a waveguide filled with a dielectric material of dielectric constant, ε_r, (see Reference 10) is given by[11]

$$\lambda_g = \lambda_o \left[\varepsilon_r - (\lambda_o/\lambda_c)^2 \right]^{-1/2} \qquad (2\text{-}5)$$

where

$\lambda_o = \dfrac{29.969 * 10^{10}\ \text{mm/s}}{\text{frequency in Hertz}}$ = freespace wavelength (mm) in air

λ_c = cutoff wavelength (mm)

= 2 * broad dimension (mm), for rectangular waveguide, or

$= \dfrac{\pi * \text{diam.(mm)}}{1.841}$, for circular waveguide.

The impedance of a rectangular or circular waveguide operating in the transverse electric (TE) mode is given by

$$Z(\text{TE}) = (\mu_o/\varepsilon_o)^{1/2}\ \lambda_g/\lambda_o \qquad (2\text{-}6)$$

where

$(\mu_o/\varepsilon_o)^{1/2} \cong 120\pi\ \Omega$ = impedance of free space

ε_o = free space dielectric constant (F/m)

μ_o = free space magnetic permeability (H/m).

If two materials of different dielectric constant are adjacent in a waveguide, part of any wave impinging on that junction will be reflected because of the impedance mismatch. To have all the microwave power propagate past the junction without reflection, a quarter wavelength matching section of a third material is inserted between the first two materials, with the provision that

$$Z_{qw}(\text{quarterwave section})^2 = \{ Z_1(\text{mat'l 1}) * Z_2(\text{mat'l 2}) \}. \qquad (2\text{-}7)$$

In early work, the impedance matching technique used a Teflon wedge. Although the wedge provided only partial matching, it was simple and did help. The dielectric constant of the packed porous bed of HMX was assumed to be near 3.0. (The actual dielectric constant for this material had not been measured at that time by us, nor reported elsewhere). Teflon was known to have a value for ε_r around 2.1, and the value for air was known to be 1.0. Therefore, solid Teflon was an intermediate valued material suitable for use as a transition section. The wedge shape of the

downstream end of the transition section allowed a smooth transition between the impedances of air and Teflon, leaving only the abrupt small change in impedance between Teflon and that of the test bed. A better match would have been achieved with a double-ended wedge, but this created problems in loading porous test beds to constant density around the wedge. Valuable insight into testing methods developed with experience, and we soon began to include quarter-wave stub matching techniques in place of the Teflon wedge.

There are many ways to find a matching material but, as will be shown, it is convenient to use a powder that can be compressed to a density resulting in the relative dielectric constant of the desired value. In this case, 55 %TMD Teflon 7C powder has $\varepsilon_r = 1.54$.[8] An 8.53 mm thick by 25.4 mm diameter cylinder of Teflon 7C is pressed in another tube, then relocated at the interface of the HMX which is then matched to air.

As an example of the equation usage, consider the problem of matching a porous bed of 73 percent theoretical maximum density (%TMD) Class D HMX in a cylindrical waveguide (25.4 mm ID) to air. HMX (material 1) of this density has a dielectric constant, ε_r, of 2.81 and air (material 2) has $\varepsilon_r = 1.00$ (Reference 12). At our frequency of 9.00 GHz, one can determine the values of the wavelength in air, λ_o, to be 33.29 mm, the cutoff wavelength in the cylindrical waveguide, λ_c, to be 43.34 mm. The impedances can be calculated from Equations (2-5,6) to be $Z_1(\text{HMX}) = 120\pi/1.487$, and $Z_2(\text{air}) = 120\pi/0.6408$. These values can then be inserted into Equation (2-7) to yield $Z_{qw} = 120\pi/0.9762$. Equation (2-6) yields $\varepsilon_r(qw) = 1.54$ from the value of Z_{qw}. This ε_r value, inserted into Equation (2-5) where the waveguide quarter wavelength can be calculated, yields $\lambda_g(qw)/4 = 8.53$ mm.

Circular Waveguide

Adaptation to circular waveguide was accomplished using rectangular to circular transition sections purchased from Systron Donner (DBG-030). These transitions output to circular waveguide at 29.2 mm ID, necessitating the fabrication of an additional transition to reach the desired waveguide diameter of 25.4 mm. Short transitions were machined from brass rod to create this

required shift in size. Copper tubing, plumbing Type "K", with 3.2 mm wall thickness, 25.4 mm ID, (nominal dimensions) is used as standard circular waveguide sections due to its availability. The cross section of this copper tubing is not perfectly constant, but the changes in cross section are not abrupt and, therefore, do not cause a problem with the transmission of the microwave power. A non-constant cross section will normally cause the production of higher order modes but, if they occur here, they will be quickly damped, as long as the frequency is kept below 9.0 GHz in this circular waveguide.

A simple design for coupling sections of circular waveguide together was devised for our size waveguide. Brass rings are soldered to the end of each copper waveguide section, and then the joint is clamped together using steel flanges. The flanges are recessed to allow the brass rings to just fit, then "*hand*" alignment of the flanges was assumed to result in proper alignment of the waveguide pieces. This was found later not to be the case; alignment pins were then included on the flanges which automatically assure waveguide alignment. These pins, shown in Figure 2-3, also serve to preserve a fixed spatial orientation for those components, such as tuners, which do not possess circular symmetry.

Right angle circular waveguide bends were incorporated to protect passive waveguide components downstream of the energetic materials and to permit microwave interfacing to vertical testing orientations. Later, straight circular sections of waveguide loaded with a low-loss powder were also added as "*damper sections*"[13] to attenuate the detonation pressure wave and further protect the expensive circular bends, rectangular-to-circular transitions, and other waveguide components. In a further effort to protect downstream parts, a short section of semi-rigid coaxial cable was inserted into the circuit within the firing chamber. This was done to add additional protection to our equipment from strong pressure waves and also to limit the propagation of unburned energetic material and inert damper material back to the circuit table outside the firing chamber.

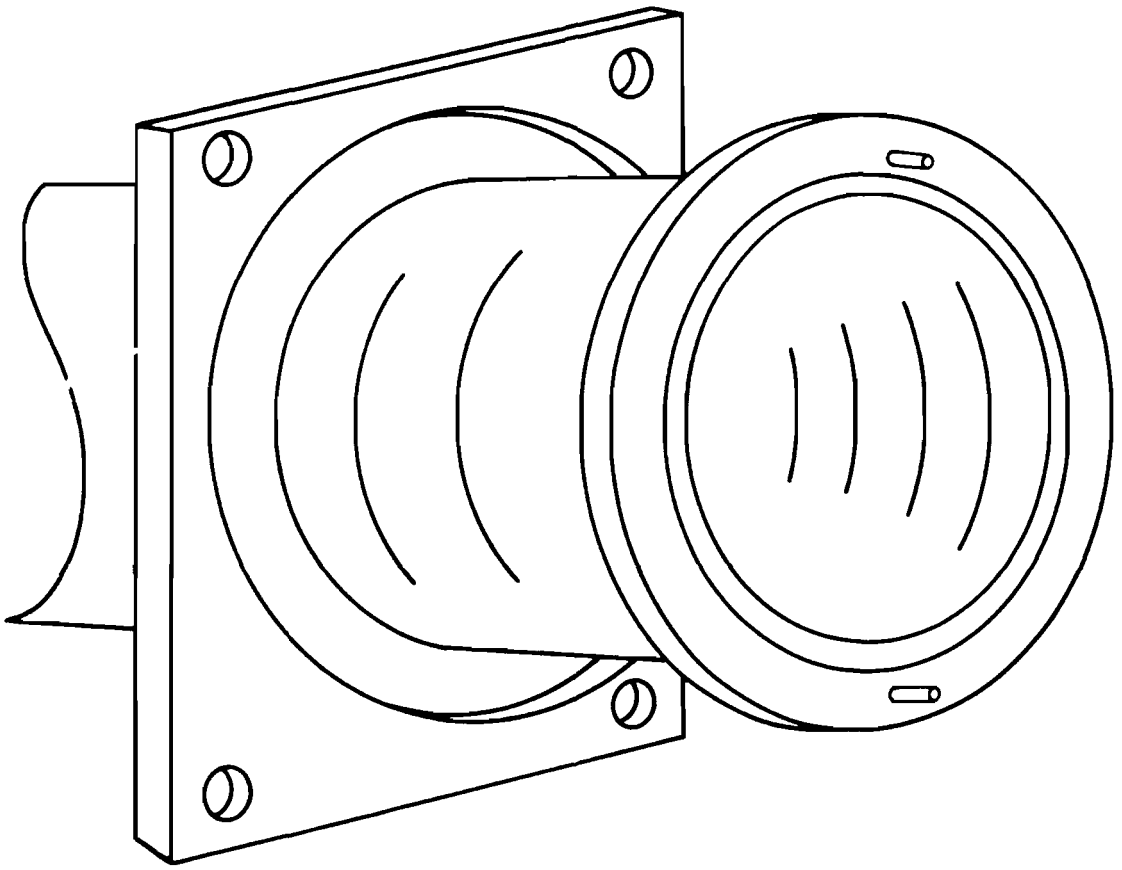

FIGURE 2-3. CIRCULAR WAVEGUIDE ALIGNMENT FLANGE SETUP WITH ALIGNMENT PINS SHOWN

CHAPTER 3

DIELECTRIC MEASUREMENTS

Introduction

Both the analysis of reflector position from interferometric output (Equation (2-4)) and impedance matching within the interferometer (Equation (2-5)) require precise values of the guide wavelength in the dielectric material, λ_g. These values are based on the relative dielectric constant (ε_r) for the material and the type of waveguide. It is the value of ε_r that relates the microwave reflection mathematically to the bed's material properties.

In a homogeneous medium the complex dielectric constant or permittivity, ε_c, is given by;[9]

$$\varepsilon_c = \varepsilon_o [\varepsilon' - j\varepsilon''] \qquad (3\text{-}1)$$

where

ε' = relative dielectric constant = ε_r

ε'' = loss factor produced by non-ideal dissipative currents

$\varepsilon_o = 8.854 * 10^{-12}$ Farads/m (Système Internationale (SI) units).

In further discussions where mention is made of dielectric constant, the reference will be to the relative dielectric constant, ε_r, unless explicitly stated.

There is little reference data for the variation of dielectric constant with variables such as density, temperature, and humidity. Although some dielectric constant measurements for energetic materials were compiled by Lawrence Livermore National Laboratory (LLNL),[12] many of the materials of interest in the present work were not available. Also, the LLNL data were not

detailed enough for our application; dielectric data are presented for a material in a range of densities at a given frequency, rather than as a value of ε_r for a specific frequency at a single density. For example, Comp B measured at a frequency of 3 GHz is reported as having a dielectric constant of 3.25 for a density between 1.6 and 1.79 g/cm^3. This sparse reporting of energetic material dielectric data was inadequate for our needs; therefore, to analyze microwave interferometer output data properly, measurements of dielectric parameters were required for materials of interest.

Automated Dielectric Measurement System

Early dielectric measurements were made at NSWC using a slotted line section with samples encased in rectangular waveguide. The accuracy of this technique was proven to be very good when standard samples were checked.[10] Unfortunately, this method is tedious and time consuming, even though the slotted line measurements are automated and the required calculation of a transcendental equation is computerized. The variation of dielectric constant with density follows an analytical mixing law, relating the volume fraction of the constituents in the bed to the dielectric constant of the mixture:

$$\varepsilon_r = \varepsilon_1^{v_1} * \varepsilon_2^{v_2} \quad \text{or} \quad \log \varepsilon_r = v_1 \log \varepsilon_1 + v_2 \log \varepsilon_2 \qquad (3\text{-}2)$$

where

ε_r = dielectric constant of the mixture

ε_i = dielectric constant of the ith material at TMD

v_i = volume fraction of the i^{th} material, percent TMD/100.

This law has been widely attributed to various authors as being empirically discovered, but was actually given a theoretical basis as early as 1931 by Lichtenecker and Rother.[14] In the case of packing a single porous material to a given density, only the term for the one material applies, since ε_2 for air is 1.0.

Measurements of dielectric constant as a function of bed density were obtained for porous Class D HMX using this method. Figure 3-1 shows a least square linear regression fit of the data which is given by the equation

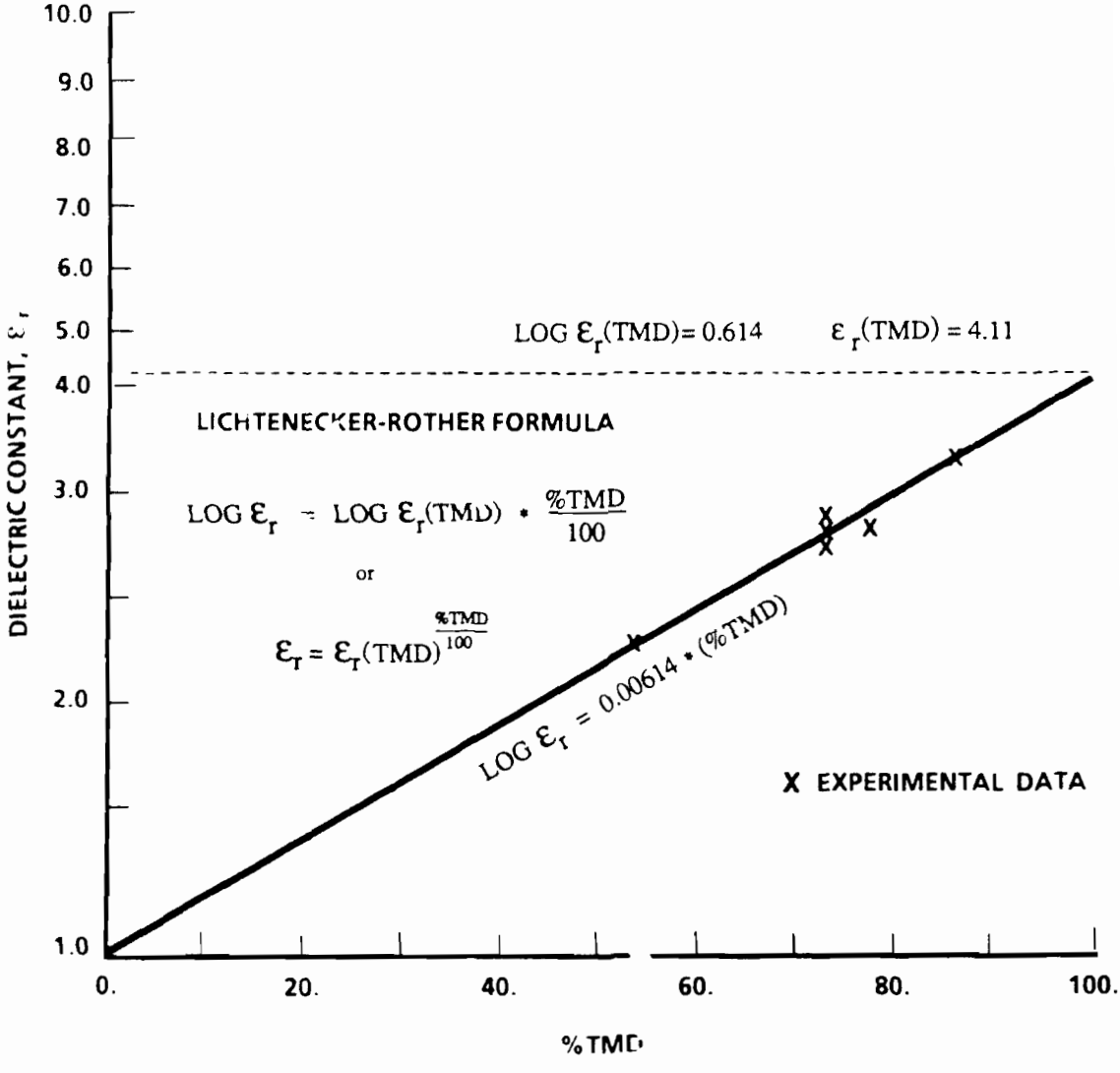

FIGURE 3-1. VARIATION OF DIELECTRIC CONSTANT WITH DENSITY FOR CLASS D HMX AT 8.3 GHz

$$\log_{10}\varepsilon = 0.00001 + 0.00614 * (\%TMD) . \qquad (3-3)$$

By inserting 100 percent, the value of the dielectric constant of TMD HMX is determined to be 4.11. This value is for a random orientation of monoclinic crystals and can be compared to a reported[12] value of $\varepsilon_r = 3.087$. Differing measurement frequencies may account for the difference in values. Similar measurements of dielectric constant as a function of bed density were obtained for Teflon 7C, melamine, and mixtures of aluminum and melamine.

Cavity Resonance Method

With the recent availability of microwave generators that have very good frequency stability and accuracy, it appeared that a cavity resonance method of measuring dielectric constant would be relatively simple and, therefore, much more acceptable to future investigators wishing to make dielectric measurements of new materials. This method involves an electromagnetic cavity which can resonate at a series of frequencies, the lowest frequency being the simplest to identify.

The cavity consists of a short, aluminum cylindrical section (length of 15.4 mm and diameter of 15.3 mm) to be used with circular waveguide. Irises of 8.4 mm diameter are matched to both ends of the transmission cavity section allowing the passage of the maximum microwave power when the cavity is resonating. For example, measuring the frequency of resonance of the empty cavity yields a resonant frequency of f_o. One then fills the cavity with the dielectric material to be tested and again measures its new resonance, f_ε. The dielectric constant (ε_r) is then given by the equation,

$$\frac{f_o}{f_\varepsilon} = \sqrt{\frac{\varepsilon_r}{\varepsilon_{air}}} . \qquad (3-4)$$

where $\varepsilon_{air} = 1.0$, the dielectric constant of the empty cavity.

The accuracy of this procedure improves with the use of standard samples having a known dielectric constant near the value of ε_r instead of air. This should provide sufficient accuracy,

given that the humidity and temperature are controlled during the measurement and subsequent testing of the materials. A small change in absorbed water vapor into the sample can make a significant dielectric variation due to the fact that the dielectric constant of water in this frequency range falls from 80 to near 40. By accomplishing dielectric measurements as well as loading in a controlled atmosphere, water vapor changes can be neglected. A slightly more involved measurement using this procedure is the determination of the imaginary or lossy part of the complex dielectric constant, ε_c. To date, we have not determined the imaginary part of ε_c, but it could be obtained, as the need arises, by taking one more measurement.

A potential problem with the use of the cavity method could arise from measuring the dielectric constant of a porous material through a range of densities. Each density of the porous material will resonate at a slightly different frequency and, thus, any variation of dielectric constant with frequency is mixed within the measurement. The waveguide slotted-line measurements are made at a single frequency, presumably the same as the test frequency. It is assumed that any variation in dielectric constant with frequency is so small in this frequency range that it can be ignored. As shown in Figure 3-2, this is the case for various materials at room temperature.[15] Unfortunately, similar data for energetic materials of interest are not available. Figure 3-2 shows representative energetic materials that have been measured at single frequencies[12] entered as data points.

In the process of making the dielectric measurements[10] of mixtures of melamine and aluminum at various densities, the value of 100 percent TMD aluminum was determined by extrapolation. Figure 3-3 shows least square fits of data from these mixture measurements. By extrapolating the data of Figure 3-3 to 100 percent TMD, these values can then be used to calculate the value of 100 percent aluminum. An average for this calculation results in an effective dielectric constant of approximately 24 for 100 percent aluminum. Although the extrapolation is from a relatively low density aluminum mixture and from relatively small particles (50 μm in this case) of random shape, it represents a method to obtain a value for the effective dielectric constant of a metal.

The electromagnetic determination of whether a material is an insulator or a metal is usually made by comparing the displacement currents to the conductive currents. The displacement currents

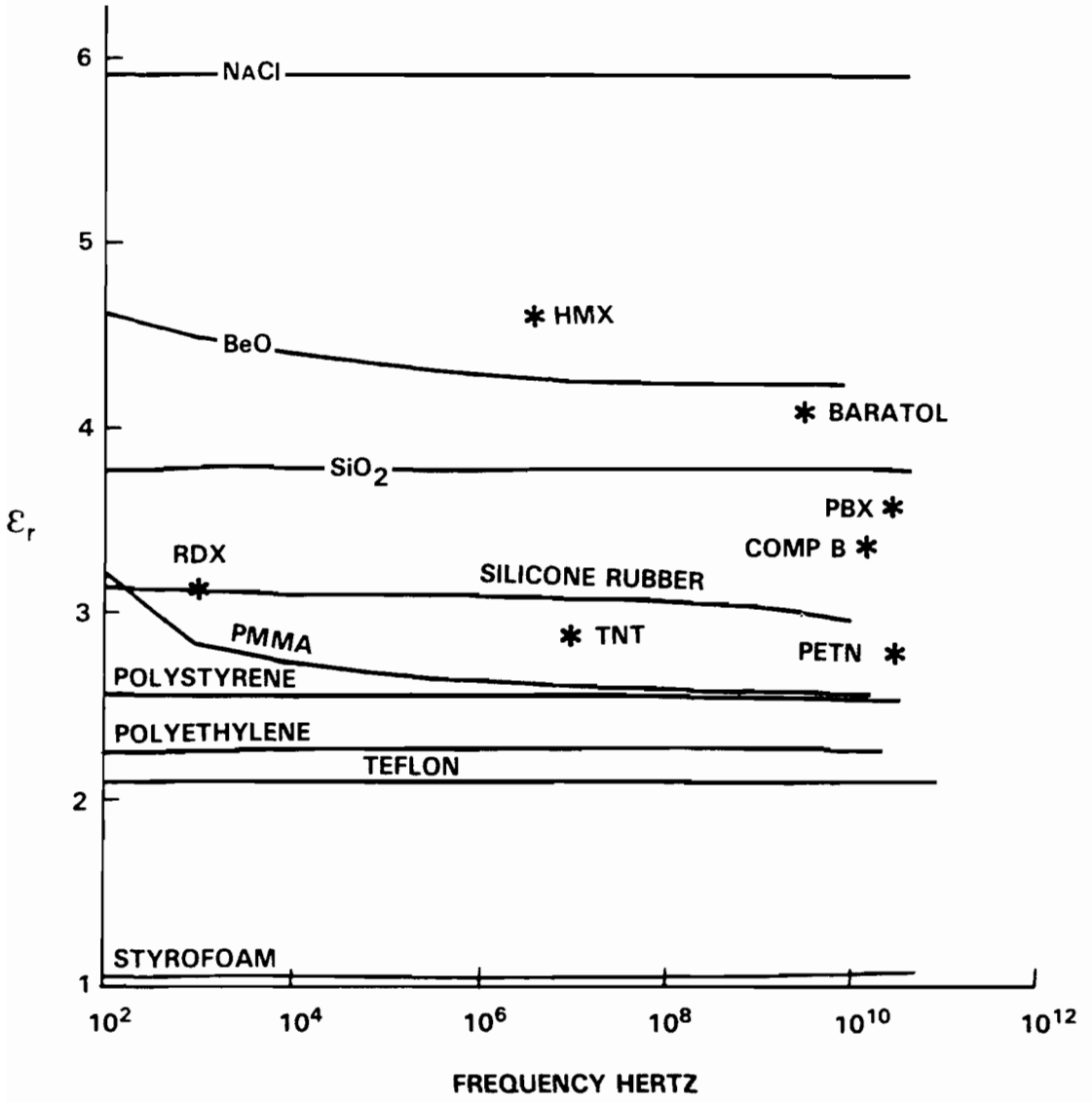

FIGURE 3-2. VARIATION OF DIELECTRIC CONSTANT WITH FREQUENCY AT 25°C (ALSO SINGLE FREQUENCY MEASUREMENTS (*) OF ENERGETIC MATERIALS)

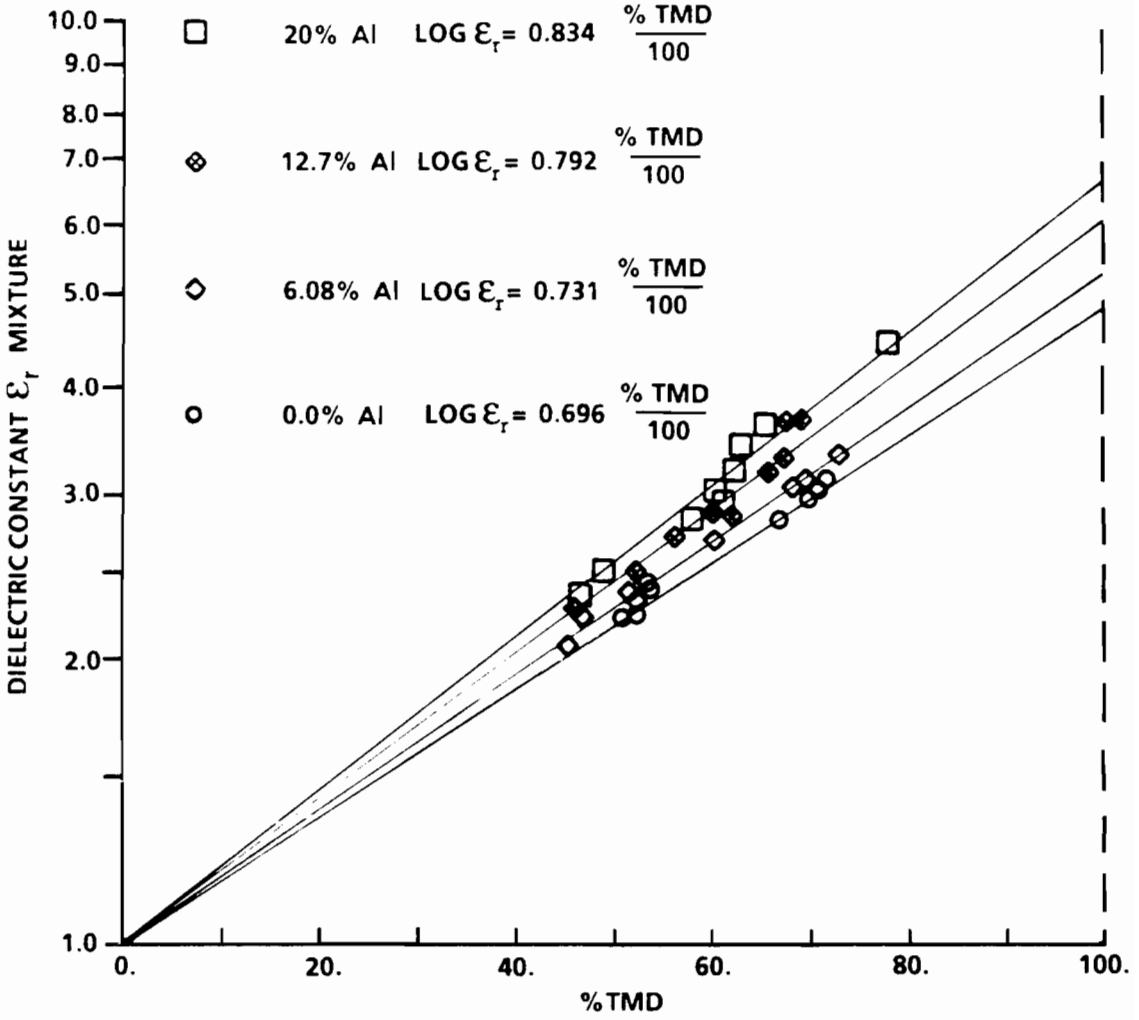

FIGURE 3-3. VARIATION OF DIELECTRIC CONSTANT WITH DENSITY FOR MIXTURES OF MELAMINE AND ALUMINUM AT 8.3 GHz

are represented as the frequency multiplied by the dielectric constant. Using a value of 24 for the dielectric constant of aluminum at a frequency of 9.0 GHz, the displacement current at $\omega\varepsilon$ = ~2 F/m*s. The conductive currents are represented by the conductivity of aluminum which is $\sigma = 4*10^7$ S. The conductive currents are 10^7 larger than the displacement currents and will therefore dominate. There is little doubt then, that the microwave reflection by aluminum is a result of conductive currents and not a dielectric discontinuity. The exact mechanism producing the microwave reflection during convective burning, compressive burning or detonation lies somewhere between these extremes of pure metallic electron density and dielectric discontinuity. Possibly a combination of these two mechanisms (dielectric discontinuity and ionization front) affect reflection in our testing.

CHAPTER 4

INTERFEROMETRIC SIGNAL ANALYSIS

In the experiments to be discussed, the interferometer has monitored the motion of one or more reflectors within the test section. The analysis of the signal from both a single reflector and two reflectors will be described, beginning with the simpler single reflector. Consider Figure 4-1 where the left side of a conductive waveguide is filled with an energetic material through which a shock (microwave reflector) is propagating. A reference plane is placed an arbitrary distance R_1 from the rightmost edge of the energetic material (the matched interface). The distance from this matched interface to the shock front is R_2. The unshocked material has a dielectric constant of ε_2, which corresponds to an internal microwave waveguide wavelength of λ_2. As the shock front moves through section 2 with velocity U, it only changes the distance R_2. At any particular instant, the distance from the reference plane to the reflector and back is $2 * (R_1+R_2)$. The total number of wavelengths in this distance is $2 * (R_1/\lambda_1 + R_2/\lambda_2)$. Since a single wavelength corresponds to 2π radians in angular rotation, the total angular rotation (Φ) for the round trip from the reference plane is

$$\Phi = 2\pi * 2 * (R_1/\lambda_1 + R_2/\lambda_2). \qquad (4\text{-}1)$$

The angular frequency (ω) is the rate of change of this total angle and can be related to the velocity of the reflector (U) by the relation

$$\omega = d\Phi/dt = 4\pi\, d(R_1/\lambda_1 + R_2/\lambda_2)/dt = 4\pi/\lambda_2\, dR_2/dt$$
$$= 4\pi\, U/\lambda_2 . \qquad (4\text{-}2)$$

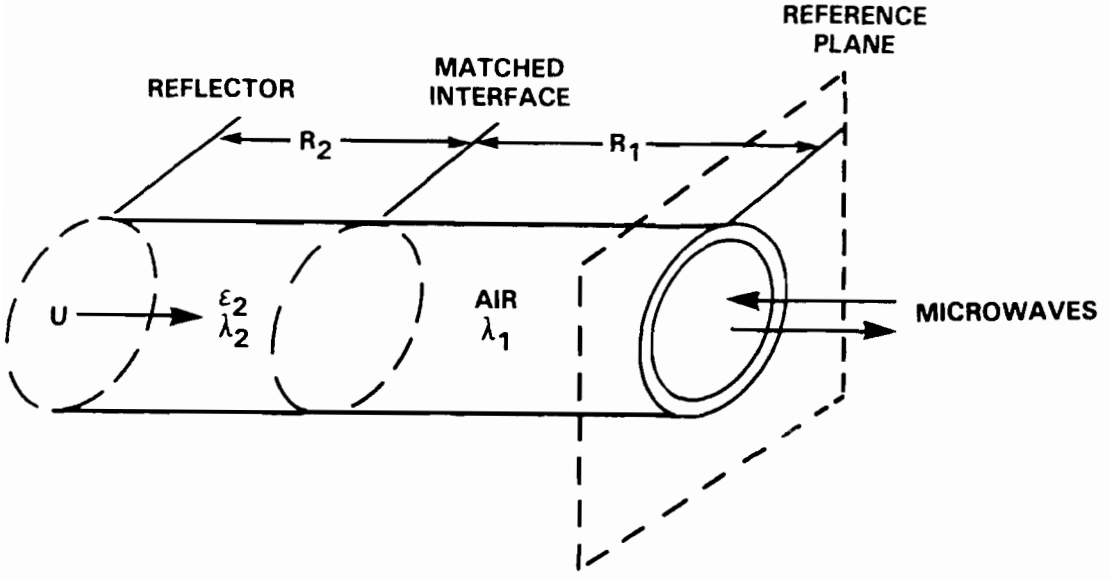

FIGURE 4-1. MODEL OF MICROWAVE REFLECTION FROM A SHOCK FRONT

The reflector velocity, in terms of the Doppler beat frequency ($f_b = \omega/2\pi$), becomes

$$U = \lambda_2 * f_b / 2 . \qquad (4-3)$$

Note in Equation (4-3) that the position of the reference plane and any material beyond the test sample has no effect on the result. Thus, any matching section has no effect except to efficiently transmit microwave power to and from the sample.

Using the shock velocity, $U = x/t$, and the period of the beat frequency, $T_b = 1/f_b$, Equation (4-3) can be reduced to

$$x = \frac{\lambda_2 * t}{2 * T_b} . \qquad (4-4)$$

Equation (4-4) was used as a simplified reduction method to analyze the locations of sine wave extremes and obtain a plot of the displacement history for the moving reflectors in the following discussions. Simple manual reduction of fringe data involves determination of beat fringe data crests and troughs for the quadrature signal and knowledge of the microwave wavelength in the dielectric material. To properly plot the displacement versus time history, one must realize that two output beats occur due to the reflecting surface displacement through one wavelength. This methodology was used in the simple analysis of the data that will be presented. Even though a plot including zero crossings of the signal and its quadrature would have yielded better spatial resolution and accuracy, the amount of harmonics combined in the output signals makes this added effort unproductive.

Velocities obtained from this simplified method are very good provided that the velocity does not change appreciably in less than half a wavelength in the material. The use of Equation (2-4) (displacement analyzed directly from quadrature data) would be required to follow large changes in velocity if they were to occur within a half wavelength.

In many of the microwave interferometric experiments, data containing more than one Doppler beat frequency have been obtained. In projectile impact experiments, a piston is accelerated to a particular velocity and then impacts a porous bed, causing a shock front to propagate ahead of the piston. The shock front as it propagates, produces a dielectric discontinuity in the bed due to

the compaction/density change. This moving dielectric discontinuity reflects a small portion of the microwave signal which is added to the larger reflection from the piston, giving the superimposed signal shown in Figure 4-2. A microwave circuit model for this case is shown in Figure 4-3. The analysis follows the same pattern as did that of the single reflector of Figure 4-1 with the addition of section 3, corresponding to the compacted bed between the shock front and the piston.

In Figure 4-3 we can assume that a waveguide section is loaded with a material sample of length ($R_2 + R_3$). A piston moving with a particle velocity u has impacted the material causing a shock wave to propagate through the sample with a velocity U. The material between the shock wave and the piston (a distance of R_3) is compressed to a high density relative to the initial density, changing the dielectric constant of this material from its original value ε_2 to a higher value ε_3.

The dielectric discontinuity between ε_3 and ε_2 at the shock front is responsible for a partial reflection that can be analyzed using Equation (4-3). The remaining majority of the signal that is not reflected passes through the shock front into the compressed region of ε_3. As it arrives at the piston, which is capped with aluminum foil, the signal is totally reflected. This piston motion imparts its Doppler shift to the reflected signal. Both the piston reflection and the shock wave reflection travel back to the quadrature detector where their output appears as superimposed beat frequencies, as can be seen in Figure 4-2. The lower frequency of Figure 4-2 is recognized as being associated with the slower moving piston. The high frequency ripple is associated with the partial reflection at the faster moving shock front.

Viewing the model in Figure 4-3, compared to that of Figure 4-1, it can be observed that the reflections from the shock front are identical. Thus Equations (4-3) and (4-4) are still valid in determining shock velocity, U. The piston velocity (assumed to represent the particle velocity) requires a modification to account for its microwave signal traveling through the region R_3 whose boundaries are both moving. This modification is given by[16]

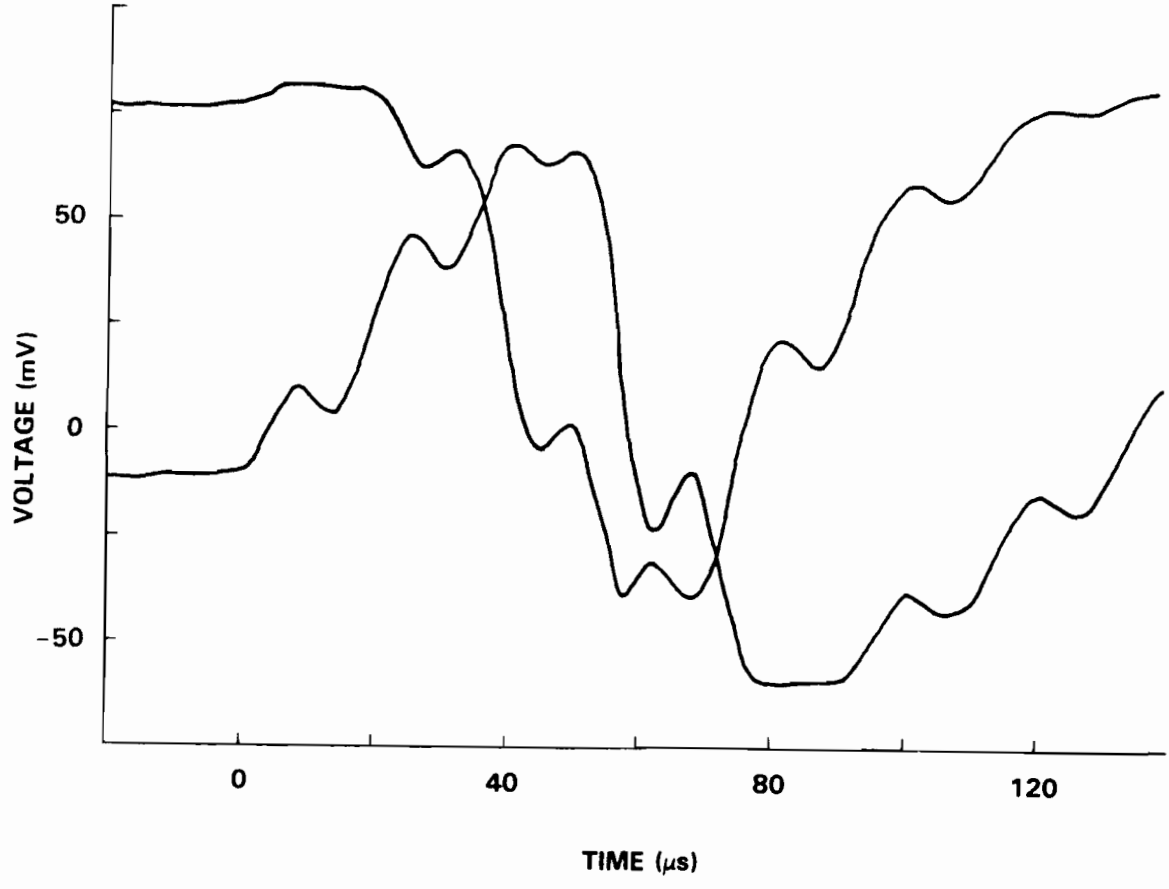

FIGURE 4-2. RAW DATA FROM PISTON IMPACT EXPERIMENT SHOWING SUPERIMPOSED FRINGES

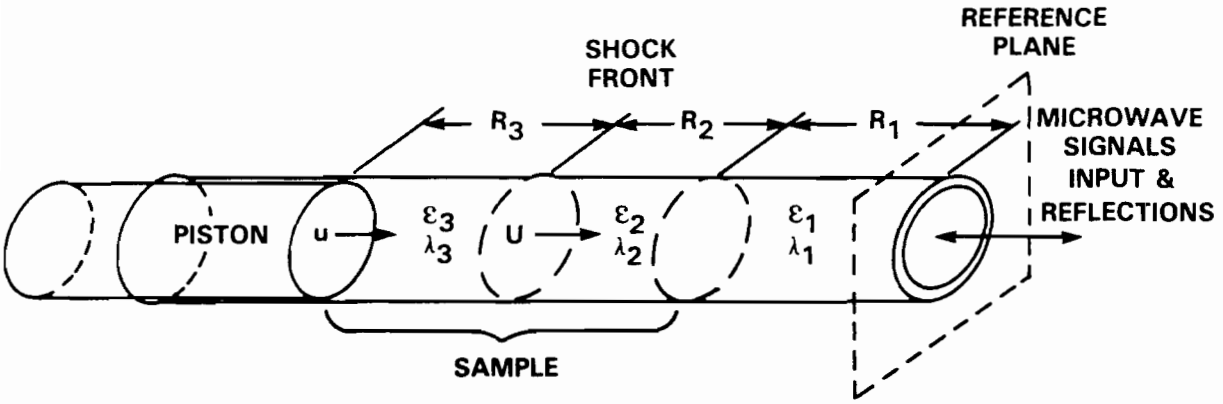

FIGURE 4-3. MODEL FOR PISTON AND COMPRESSIVE WAVE REFLECTIONS

$$u = \left(\frac{U}{\lambda_2}\right) * \left(\lambda_2 - \lambda_3\right) + \left(\frac{f_p \lambda_3}{2}\right), \qquad (4\text{-}5)$$

where f_p is the beat frequency due to the piston; the remaining symbols maintain their previous definitions. Using this analysis, a reduction of the superimposed fringes from their respective regions can be obtained. It has been found that the piston velocity derived from the microwave data corresponds well with the piston velocity determined using the more conventional method of streak photography.

We have described the operative mechanism for the reflection of microwave energy as a discontinuity in dielectric constant. Also, we have discussed the reflections that occur due to the foil covered piston face, where total microwave reflection is produced by the conductivity or the density of free electrons in the aluminum. We have not, however, ruled out the possibility that an ionized front of minimal charge density is also a microwave reflector in the case of building reaction. It is yet to be determined what the true mechanism of reflection is within the reacting front.

CHAPTER 5

INTERFEROMETRIC MEASUREMENTS FROM VARIOUS ARRANGEMENTS

Simple Detonation Velocity and Detonation Transfer Experiments

This section will describe experimental arrangements used in the development of the microwave interferometric technique and various measurements obtained. All developmental testing used porous Class D HMX loaded at 73.0 percent TMD (1.387 g/cc) as the material being monitored, or as the shock driver in inert compaction tests to study shock attenuation through the inert media. HMX was also used in two detonation transfer experiments which used a section of NaCl between two lengths of the HMX.

In the earliest experimental development, the test sample consisted of a rectangular waveguide section, 10.2 mm x 22.9 mm (0.400 in x 0.900 in), loaded with Class D HMX. The microwave interferometric circuit was terminated by this waveguide section. An RP-80 detonator was used to initiate reaction within the test bed. The technique for impedance matching in these early shots was to use a Teflon wedge, as shown in the setup of Figure 5-1, for reasons stated earlier.

Resulting output fringes for this test are shown in Figure 5-2. These raw data are indicative of many of the early tests where a baseline shift in the output fringes occurred at early times. The baseline shift is most likely due to the arbitrary placement of the short at the end of the waveguide section. The fringes will naturally tend to the center of the beat signals, regardless of their amplitudes. This could be eliminated through the use of a phase shifter in the input leg of the interferometric circuit (one has not been readily available for our use to date). It can be seen from these data that a very constant frequency of output fringes was obtained. Constant frequency fringes indicate a steadily moving reflection front and, in this case, the reflection front was a steady state detonation of the energetic material. Using manual reduction procedures on these fringes, a plot of displacement versus time of the

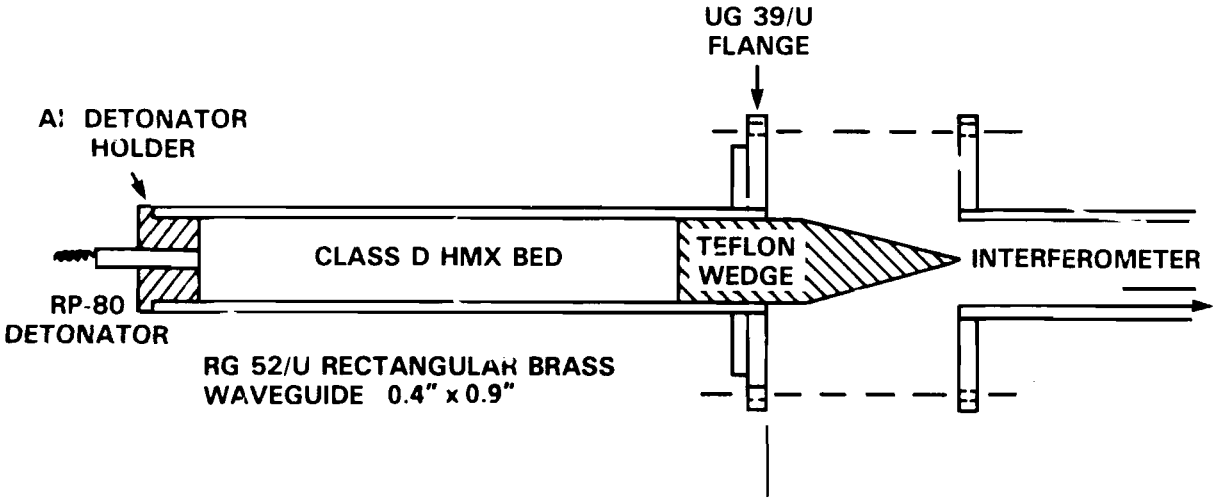

FIGURE 5-1. RECTANGULAR WAVEGUIDE SETUP WITH TEFLON WEDGE AS MATCHING SECTION

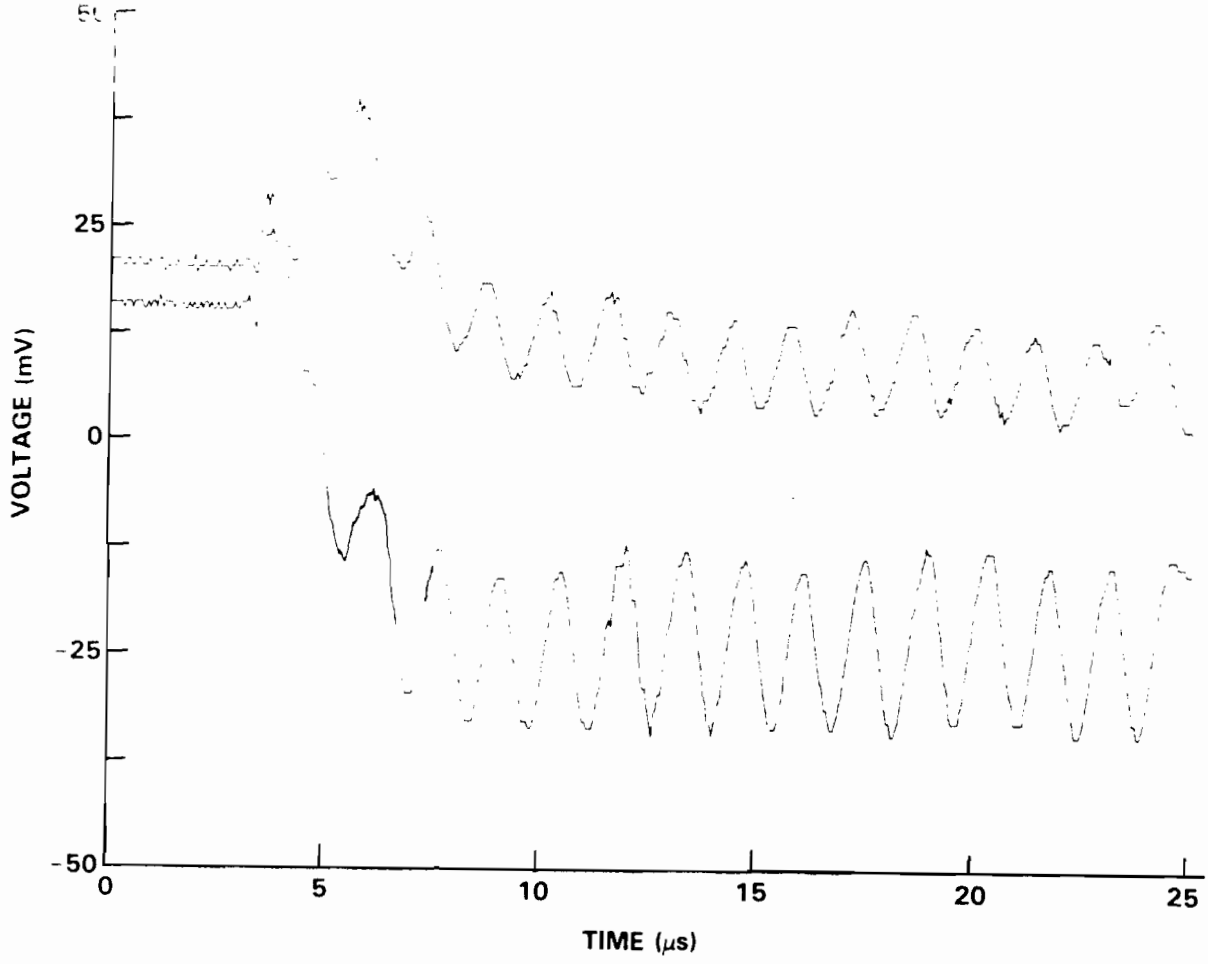

FIGURE 5-2 OUTPUT FRINGES FROM RP-80 INITIATED DETONATION OF 73.0% TMD CLASS D HMX WITHIN RECTANGULAR WAVEGUIDE

propagating detonation wave was determined as shown in Figure 5-3. The velocity of the detonation front was determined to be 6.63 mm/μs, comparing well with other experimental results obtained from Lexan tube confinement of detonating Class D HMX.

Two other early tests in rectangular waveguide involved composite HMX-NaCl samples. A steady state detonation was initiated in a section of 73.0 percent TMD Class D HMX, loaded at 1.387 g/cc, then attenuated through a section of NaCl (1.285 g/cc, 59.4 percent TMD) with SDT then observed in a second section of Class D HMX, again loaded at 73.0 percent TMD. NaCl was chosen as a material that would exhibit a good deal of ionization as a shock wave passed through its length (it had been postulated that ionization was required for reflection to occur). A piece of 0.003 in Al foil was loaded 25.4 mm away from the detonator in the first bed of HMX to allow the early detonation wave to become steady before passing through the foil and reflecting the microwave signal.

Figure 5-4 shows raw data for M-7, the first of these two similar tests, and Figure 5-5 shows the displacement versus time histories of the two tests compared. A prominent and interesting phenomena was encountered. Detonation of the first HMX bed appeared to be not promptly initiated by the RP-80 detonator. The microwave data seem to indicate that a shock wave preceded the onset of detonation, well beyond the aluminum foil loaded 25.4 mm into the HMX in both tests. The evidence for this is the increased detonation velocity in the early section of the test bed; the detonation wave slows at the point where the detonation wave would have overtaken the compaction wave and entered the lower density region. This, though, could also be due to a reflection from the aluminum foil, associated with the diverging wave front passing through, causing a misinterpretation.

A repeat of experiment M-7 showed this phenomena to be attributable to the test itself and not an artifact of the test. In both cases, propagation of the shock through the NaCl bed was clearly visible, indicating that the interferometer could be used to monitor a shock propagating through this inert material. This supported the hypothesis that ionization was contributing to the microwave reflection but did not discount the possibility that reflection might be due either to the compaction occurring with the passage of the shock front or, possibly, a combination of the two.

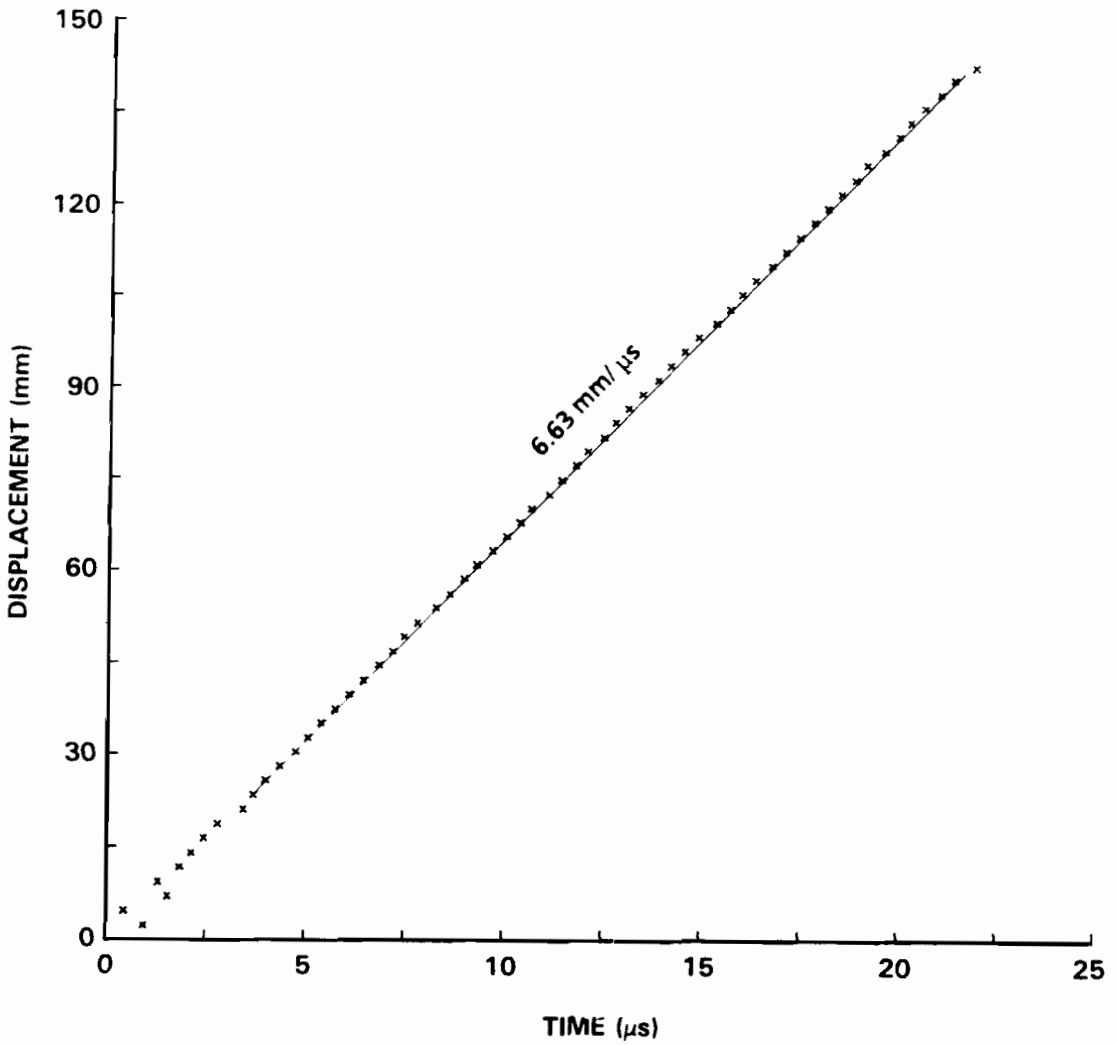

FIGURE 5-3. DISPLACEMENT VERSUS TIME FOR RP-80 INITIATION OF DETONATION IN CLASS D HMX IN RECTANGULAR WAVEGUIDE

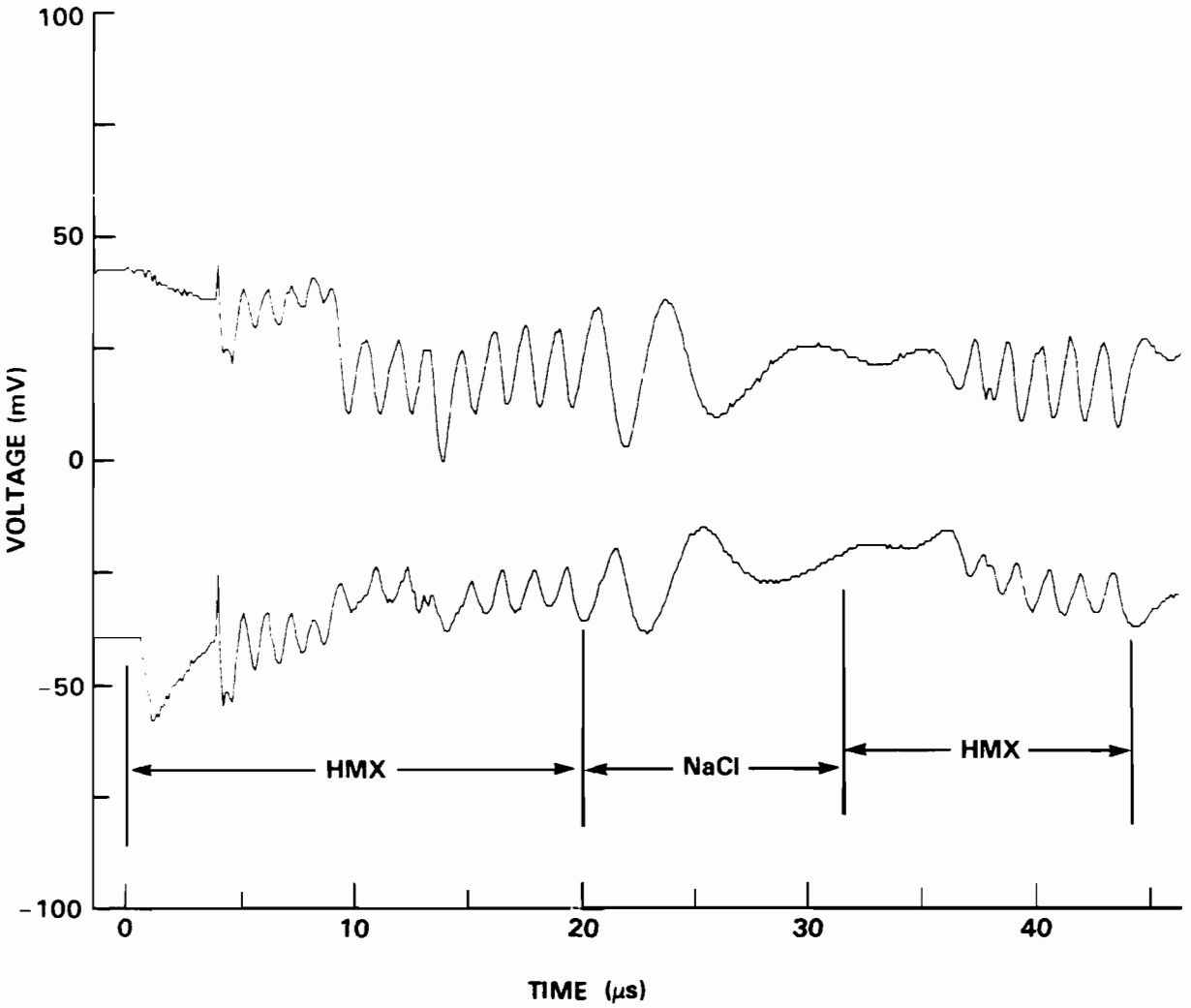

FIGURE 5-4. OUTPUT FRINGES FROM DETONATION TRANSFER TEST, M-7, USING COMPOSITE BED OF HMX/NaCl/HMX

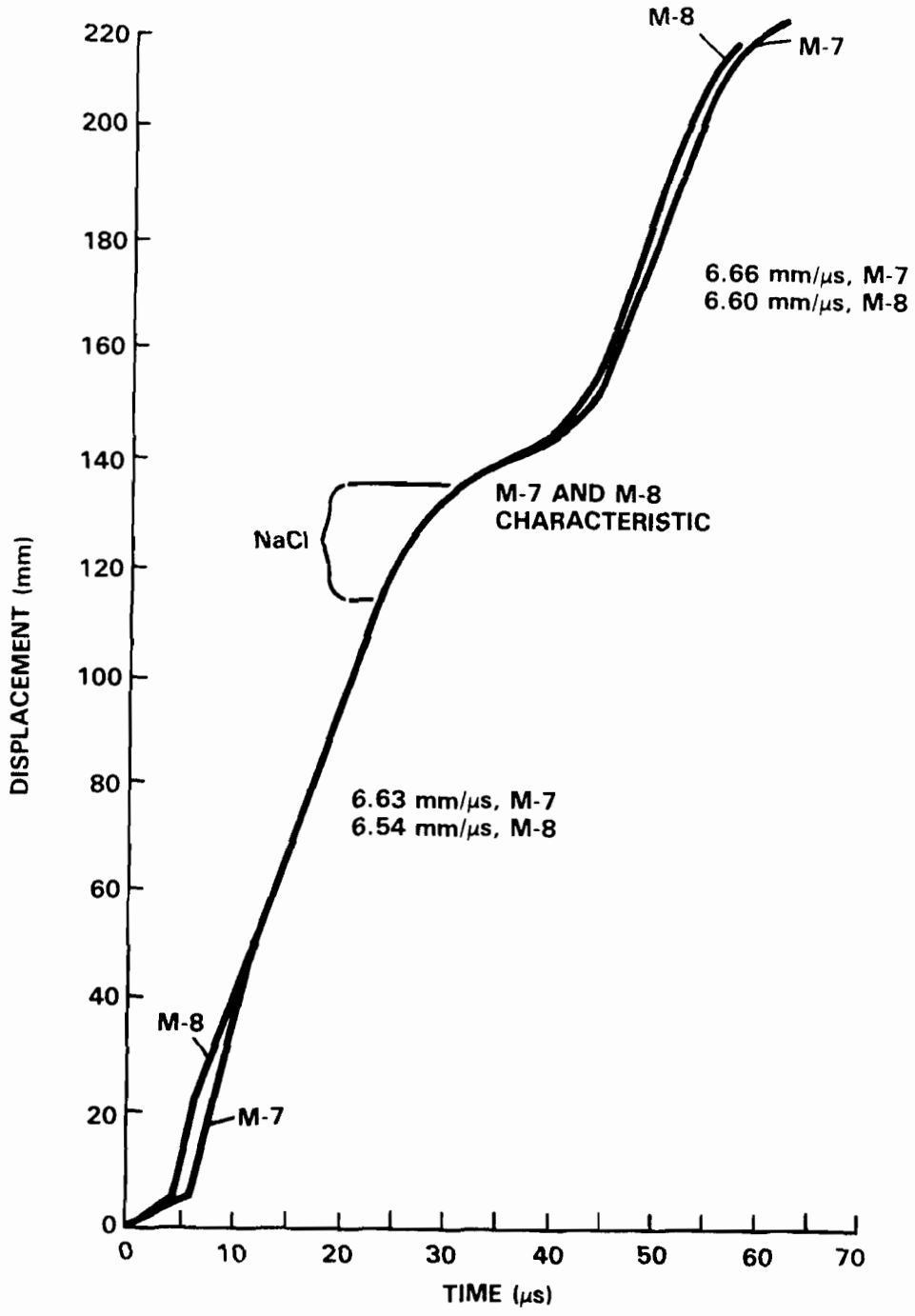

FIGURE 5-5. DISPLACEMENT-TIME HISTORY COMPARISON OF TWO HMX/NaCl/HMX DETONATION TRANSFER TESTS

Shock Wave Reflections

Tests were run to further our understanding of the compaction wave strength necessary to reflect the microwave signal within an inert, presumably non-ionizing, material. These tests consisted of a detonating bed of Class D HMX driving a shock wave into a length of porous Teflon. In the first test, both a detonation front (velocity of 7.14 mm/μs) in the 76.2 mm section of 73.0 percent TMD HMX and the shock wave in the 133.2 mm section of 60.0 percent TMD Teflon 7C were monitored by the interferometer. The shock velocity slowed to 0.90 mm/μs before the recording period of the instrumentation ended. The raw data of Figure 5-6 show that the output fringes for the detonation wave from our circuit were undergoing a baseline shift. If a compaction wave in the HMX is assumed in this case, then fitting a sine wave through the data and using Equation (4-3) reveals that the velocity would be approximately 0.40 mm/μs. This estimated compaction front velocity compares favorably with the velocity one expects for a low amplitude compaction wave in Class D HMX.[17] Also note that the measured velocity of the detonation front is higher than expected for the initial density of 73.0 percent TMD Class D HMX; the higher velocity supports a pre-compacted bed postulate.

A second test was run using the same arrangement to explore further the compaction strength necessary to reflect microwaves. This time, though, a piece of aluminum foil was placed within the bed of Teflon 7C, 38.1 mm from the HMX/Teflon interface so that all reflections would hopefully be from the Teflon bed. If the shock front were weak enough to reflect only a portion of the signal, the remainder would be reflected from the aluminum foil moving at the particle velocity of the porous bed, and the two signals would be superimposed. No evidence of superimposed waves was observed in the output of this test; therefore, no direct information could be deduced to separate the particle (foil) velocity from the compaction front velocity. Although the recorded waveform was not smooth nor easy to analyze, use of Equation (4-4) indicates that a front could be followed for ~100 mm (or 70 μs) into the Teflon. The computed velocity was approximately 0.16 mm/μs originally, and slowed to a nearly constant velocity of about 0.05 mm/μs. It is evident that these data represent the particle velocity and not the compaction velocity. The compaction front signal superimposed on the reflection from the aluminum foil was evidently not of sufficient strength to be seen above the compaction signal or other noise.

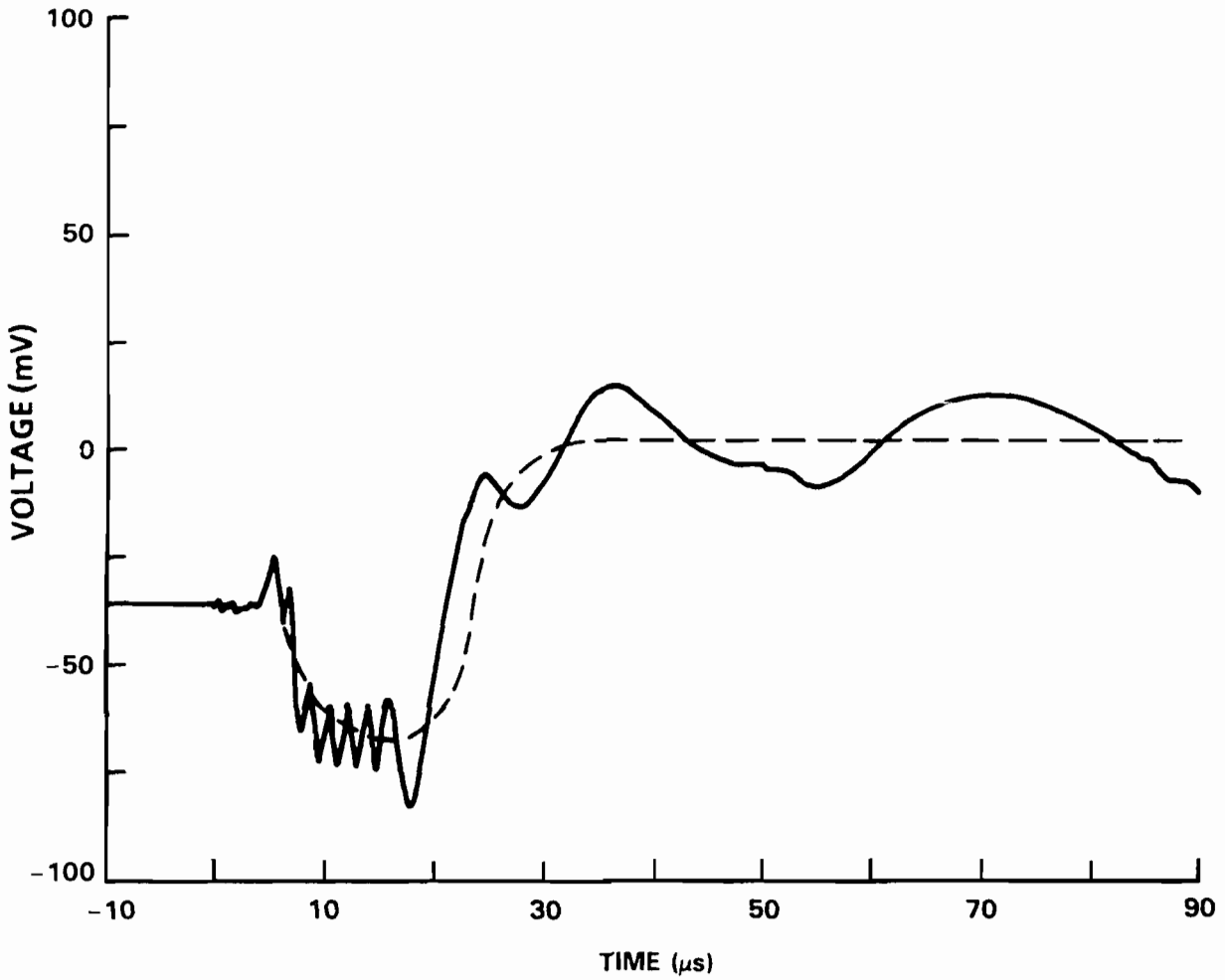

FIGURE 5-6. OUTPUT FRINGES, SHOWING DC SHIFT, FROM HMX EXPLOSIVE SHOCKING TEFLON 7C

In further testing, a 30 percent aluminized inert sample was tested to simulate a "*worst case*" for the testing of aluminized energetic material. Melamine was chosen as the inert to which aluminum particles of 200 μm diameter were added. Figure 5-7 depicts the experimental test section assembly and shows a new impedance matching section which utilized a one-quarter wavelength matching plug. Raw data for this test are shown in Figure 5-8. The associated reduced displacement versus time data are given in Figure 5-9. The raw data of Figure 5-8 show that a steady detonation began as early as 4 μs, following a short process which appears again to be compaction of the bed. From the reduced data of Figure 5-9 the velocity of this detonation wave is seen to have a constant value of 6.21 mm/μs. The HMX section was loaded 76.20 mm in length, implying that the detonation transited the HMX in about 12.3 μs, or that the shock arrives at the inert at about 14.5 μs (including a delay for initiation of the RP-80 detonator. After this time, the raw data of Figure 5-8 indicate that the Doppler period is increasing, and that the shock wave is slowing as it transits the aluminized inert. This is also quite evident in Figure 5-9 where the slope (velocity) of the curve decreases to a value of 0.53 mm/μs at about 100 μs. These experiments demonstrate the technique to be useful for even this severe case of an energetic material containing 30 percent aluminum with only an "*inert*" shock propagating within.

Gap Type Experiments

The interferometric circuit was adapted to the arrangement of a gap test. The setup with the microwave interface is shown in Figure 5-10. Several tests were completed in which the velocities obtained from both streak camera records and microwave data agreed within experimental error (3 percent). The output of raw test data from the first of this type of test on Type "A" Fluid ball powder is shown in Figure 5-11. For this experiment, a layer of aluminum foil was placed between the donor explosive and the polymethylmethacrylate (PMMA) gap material in order to monitor the pressure wave propagating through the PMMA. The raw data in Figure 5-11 show interference noise from the pulse output of the power supply, then more noise from the actuation of the detonator. Low amplitude reflections cause fringes to become evident in the PMMA only as the shock wave passes through the final several millimeters. After a slowly increasing amplitude and frequency, a ringing noise is seen in the signal (also seen in other experiments), corresponding to the onset of detonation in the acceptor charge.

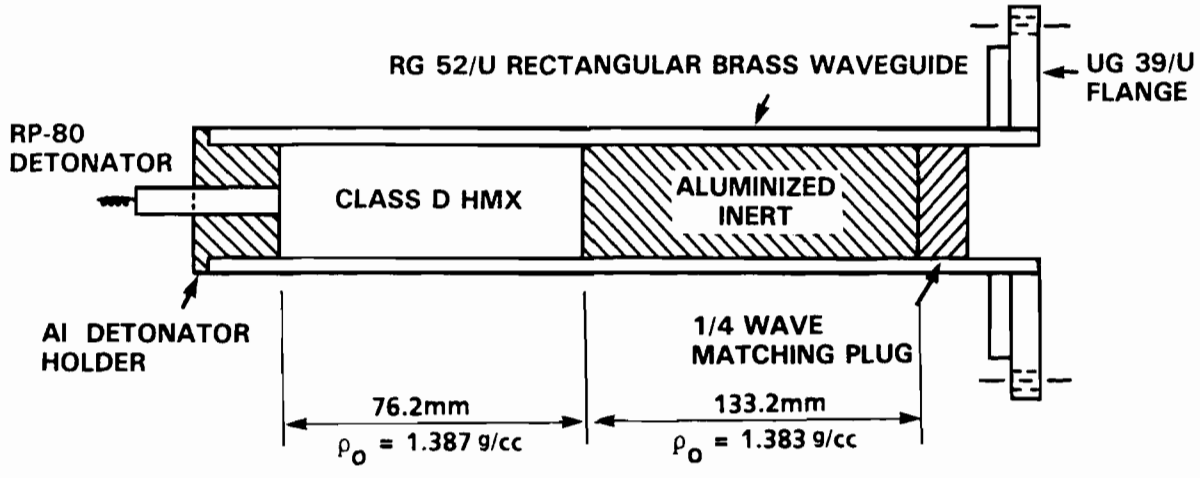

FIGURE 5-7. TEST SECTION, SHOWING USE OF 1/4 WAVE MATCHING PLUG, FOR CLASS D HMX EXPLOSIVE SHOCKING ALUMINIZED INERT

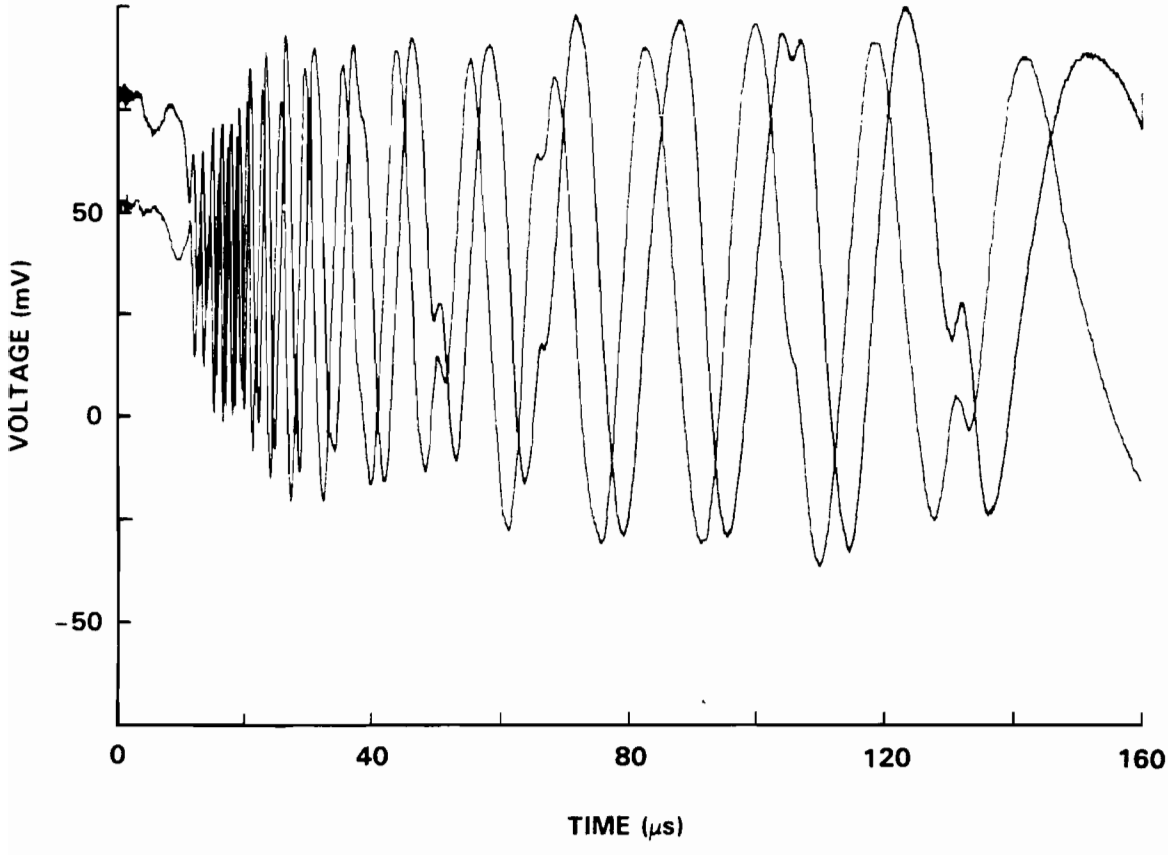

FIGURE 5-8. OUTPUT FRINGES FROM CLASS D HMX EXPLOSIVE SHOCKING 30% ALUMINIZED MELAMINE IN CIRCULAR WAVEGUIDE

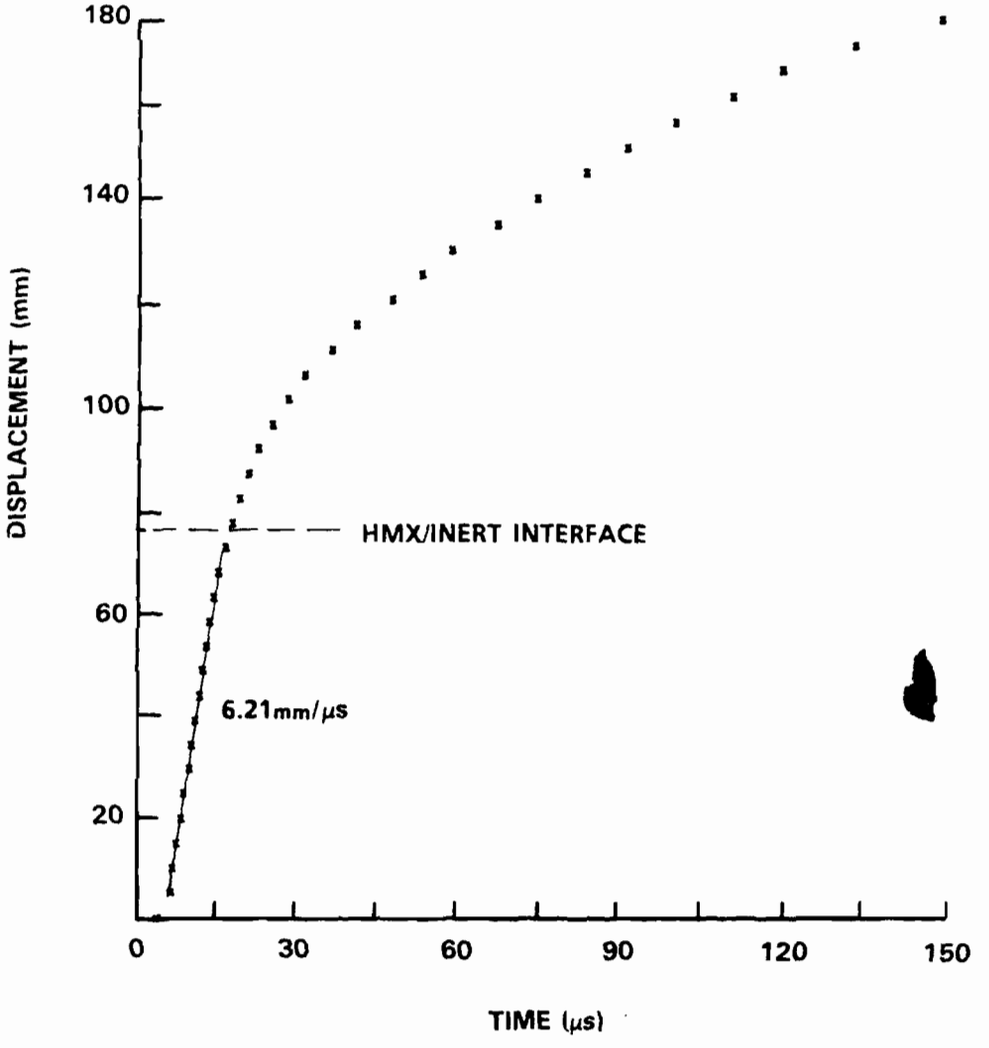

FIGURE 5-9. DISPLACEMENT-TIME HISTORY OF EXPLOSIVE SHOCKING 30% ALUMINIZED MELAMINE IN CIRCULAR WAVEGUIDE

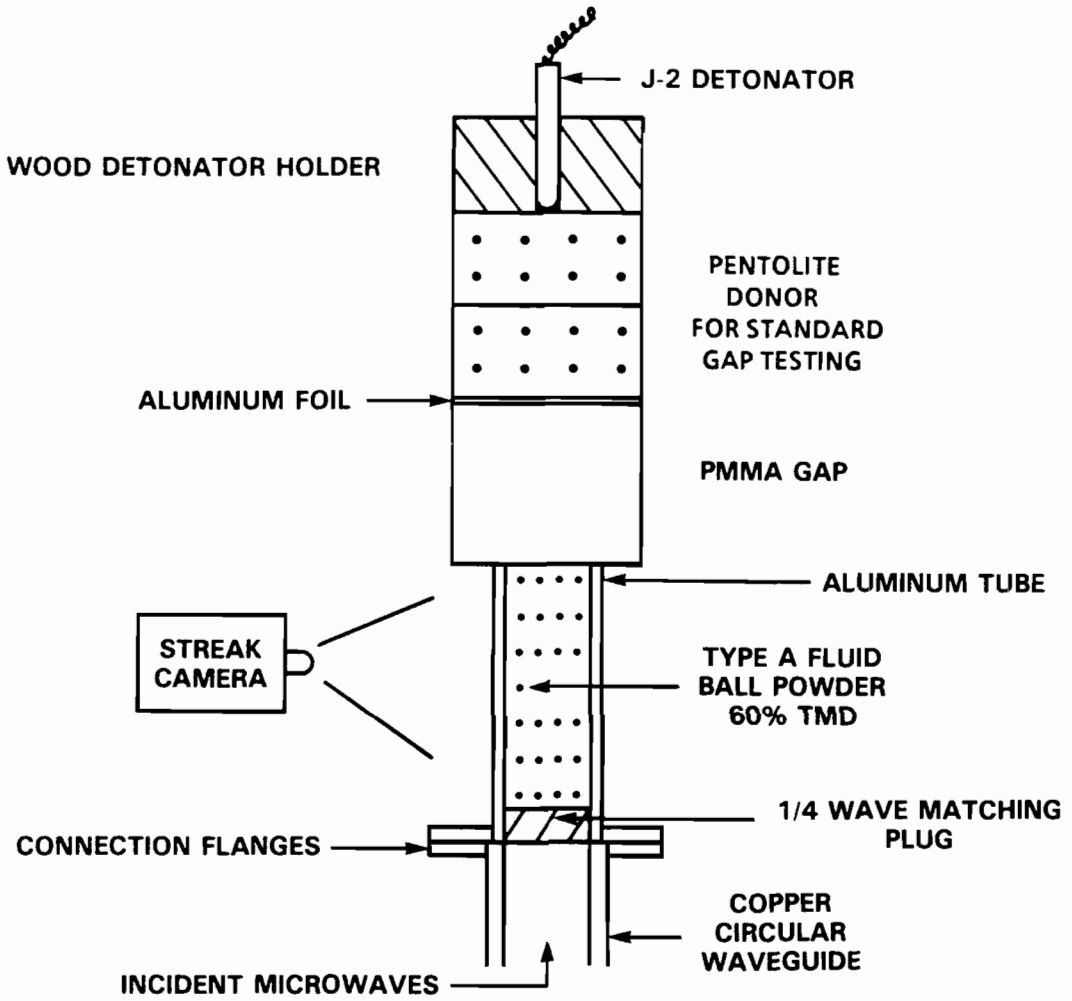

FIGURE 5-10. SETUP FOR A GAP EXPERIMENT, INTERFACED WITH MICROWAVE INTERFEROMETER

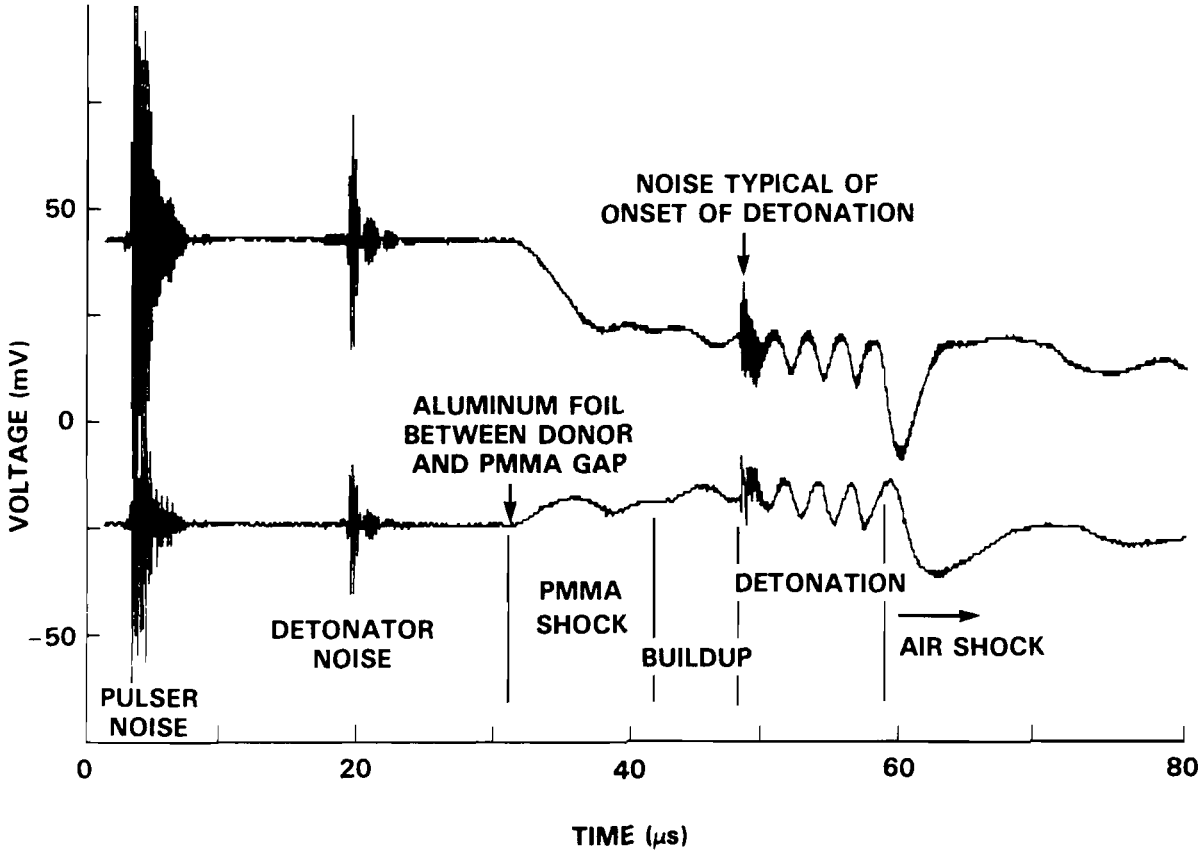

FIGURE 5-11. RAW DATA FROM TYPE "A" FLUID BALL POWDER GAP TEST

Figure 5-12 shows that the comparison between the streak camera and the microwave displacement-time data is not exact, but agrees very closely. The differences can be accounted for by the variation in the measurement methods. Camera observations look at the exterior of the charge and therefore see only the motion of the waves as they reach the exterior surface; hence, additional time for the transit of a shock wave through the wall of the confinement tube is required. The microwave system, on the other hand, looks through the interior length of the bed and averages the reflection over non-uniform surfaces (curved fronts). The discrete microwave data (~3 mm resolution) are thus seen to lead in time the continuous camera data obtained from the exterior.

Review of this gap experiment revealed that little reflected microwave signal was detected as the shock wave traveled through the PMMA. In a 1965 paper by E. Johnson,[4] it was stated that the propagation of the shock front in their plexiglass gap material in a similar arrangement had been recorded. This may be a function of the gap material used and how well the materials were impedance matched. A reflection from the shock wave in our gap material (presumably non-ionizing) would be of interest in view of a paper by Anicin, et al.[18] This paper minimized the importance of high electrical conductivity as being responsible for the reflection of microwaves. Since this view is not shared by all workers[1,3,6,7] in the field, it was decided that the gap test would be redesigned to enhance any microwave reflection that might occur during the passage of the PMMA shock wave. A large portion of the microwave power that had entered the PMMA could have easily radiated through the non-conducting sides in the first test. Consequently, the little signal that was reflected most probably would have been lost due to the physical size difference between the PMMA and the waveguide. Also, impedance across this interface was not matched, causing some power reflection at the junction of the gap material and the test bed, further reducing the return signal from this region.

The material in the next test was again Type A Fluid ball powder, with the addition of a conducting foil layer wrapping the sides of the gap material. This was intended to allow the microwave signal within the PMMA to exit only back into the interferometer. In this test, there was little, if any, improvement in the fringe signal obtained from the propagation of the shock wave through the PMMA gap. These results are most likely due to the dielectric discontinuity of the gap/acceptor

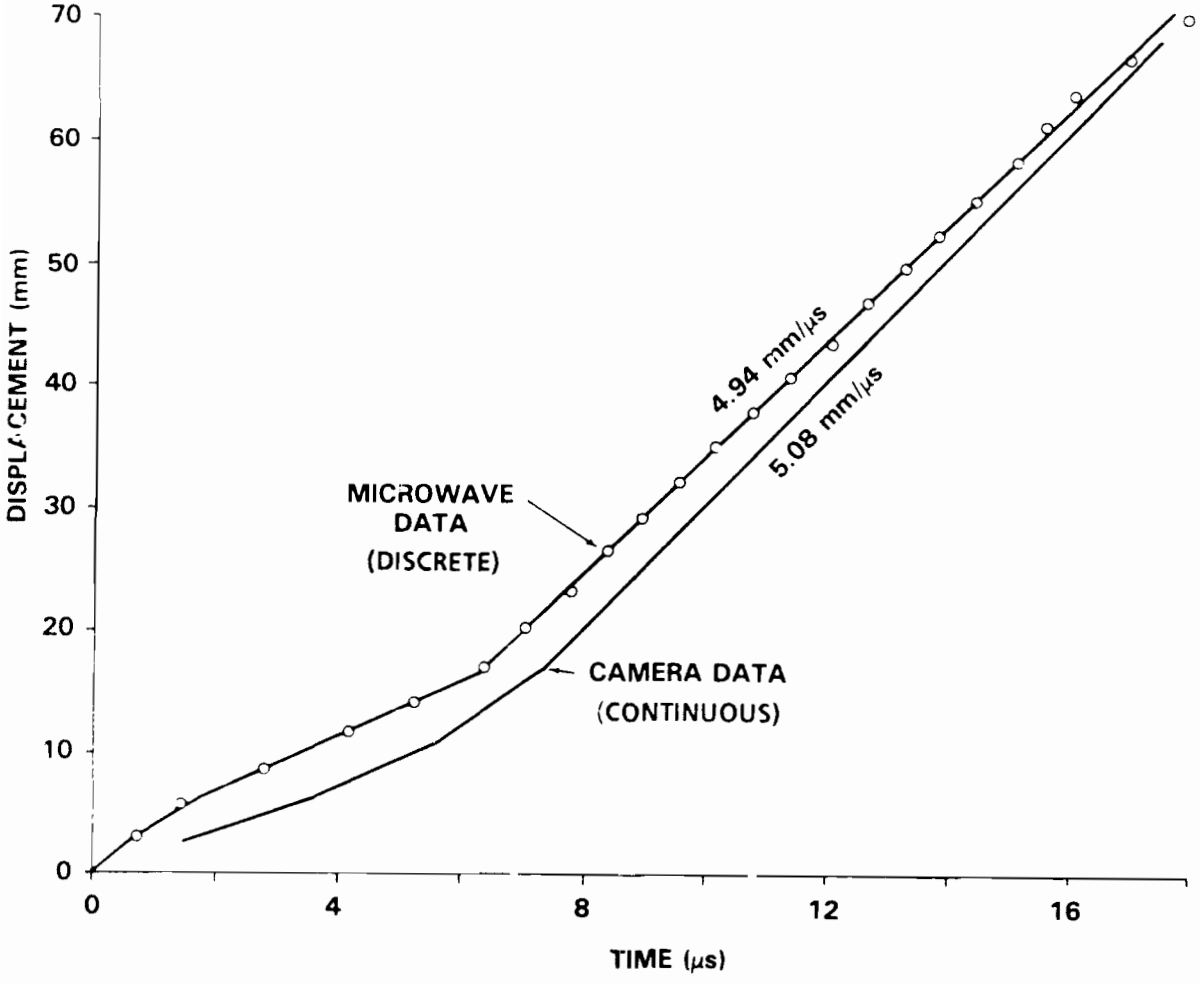

FIGURE 5-12. COMPARISON OF CAMERA RECORD WITH INTERFEROMETRIC DATA FOR GAP EXPERIMENT OF FIGURE 5-10

interface, and also possibly to the multiple reflections within the PMMA from the conductive walls. As expected, the fringes for the buildup to detonation data in the acceptor were almost identical to the previous test.

Continuing with gap type experimentation, a change to 65.0 percent TMD Class D HMX as the acceptor material provided a perfect microwave impedance match between the PMMA gap and the acceptor bed; this should increase any reflections of the shock in PMMA. Aluminum foil was again used to surround the PMMA and thereby maximized the chance of detecting shock wave reflection within the gap material. In the raw output for this test, shown in Figure 5-13, expanded around the area of interest, one can see the increased reflection of the shock passing through the PMMA. This observation confirms that in the previous gap experiments very little microwave power penetrated into the PMMA and back out through the unmatched PMMA/acceptor interface.

In this HMX gap experiment (with the impedance matched interface) a reflection was observed traveling through the entire length of the gap material, which appeared to be the shock front. A superimposed "*arbitrary shift*" was again observed in the data. This test demonstrated that shocks in solid materials can be monitored when the circuit is adequately matched to the test sample. Here, it is reasonable to expect a small dielectric discontinuity to be present in solid PMMA under these high pressure shock loading conditions; ionization associated with the shock front is not as likely. Since the initial dielectric constants of the porous bed and the PMMA were identical, the amplitude of the reflection in the PMMA gap of Figure 5-13 indicates that the reflecting discontinuity in the PMMA was greater than the discontinuity which occurred in the compression of the 65 percent TMD porous explosive bed. Alternatively, it is possible that ionization is responsible for the reflection in the compressing PMMA. For this experiment then, a dielectric discontinuity in the gap material would seem to not be the sole reflecting mechanism.

Fringe data from the HMX gap experiment show that the shock velocity through the PMMA is rapidly slowing from the detonation velocity of the pentolite donor as the pressure is attenuated by the gap. The raw data of Figure 5-13 show that SDT was attained in the bed of HMX. The data also show the propagation of an "*air shock*" in the waveguide beyond the energetic bed. Because of its large amplitude, this air shock reflection may be due to the gross discontinuity of the open circuit caused when the waveguide is destroyed following the passage of the strong shock front.

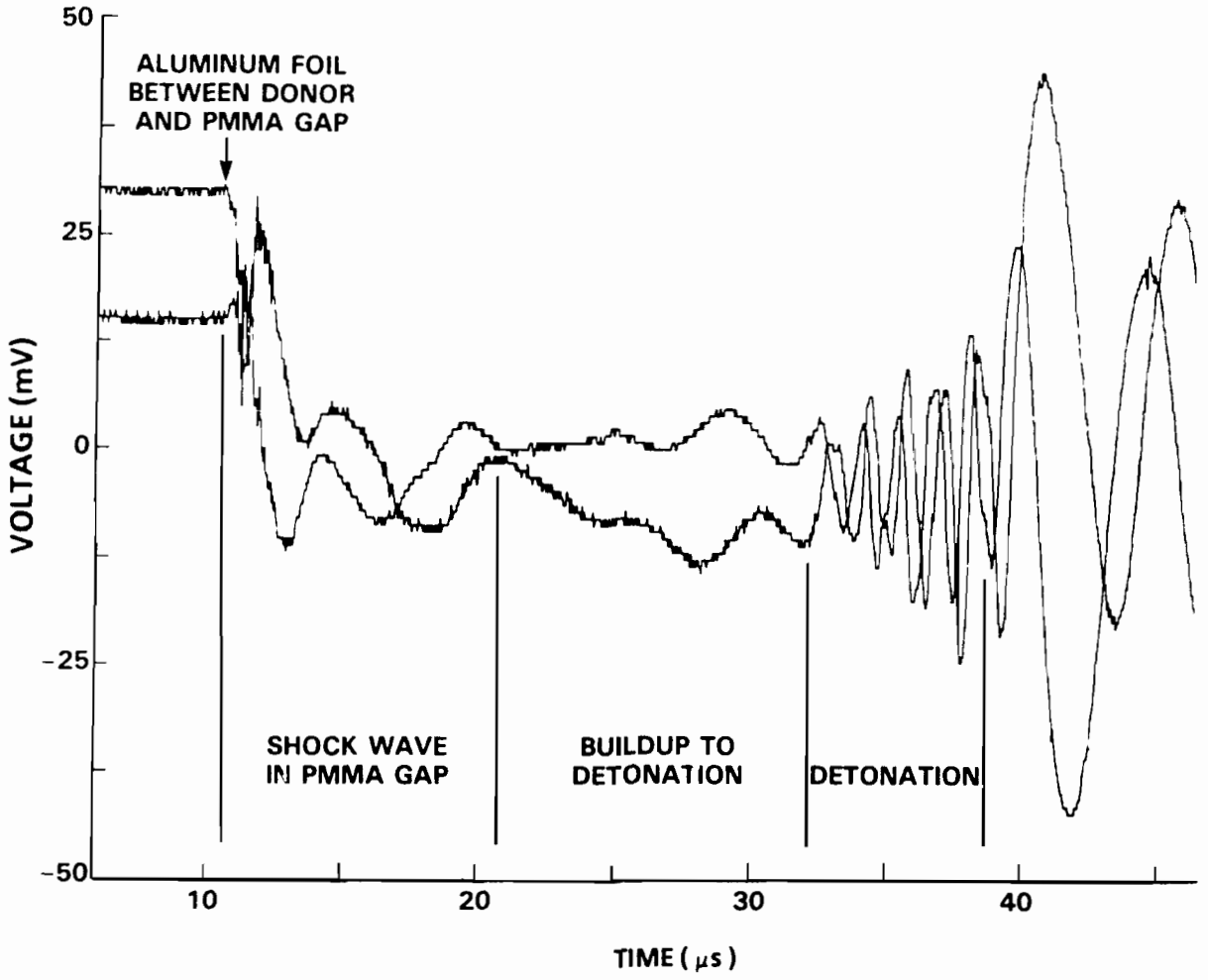

FIGURE 5-13. RAW DATA FOR 65% TMD CLASS D HMX GAP EXPERIMENT, IMPEDENCE MATCHED

Piston Driven Compaction Apparatus Testing

A microwave circuit interface for the piston driven compaction (PDC) apparatus[17] was developed as shown in Figure 5-14. This apparatus is used to simulate the final stages of DDT (compressive reaction, and SDT) by propelling a long piston into a porous bed. The piston impact maintains an approximately constant pressure up to 200 MPa for times as long as 200 μs, depending on the piston length, sound speed of the piston material, and the propelling charge. The microwave interface allows injection of the incident microwave signal through the downstream end plate. The signal is reflected off the surface of the piston, which is either aluminum or aluminum-faced Lexan, with nearly 100 percent reflection. Any reaction zone or dielectric discontinuity (shock front in this case) within the test bed will also cause a reflection of a portion of the microwave signal at its location.

The bed, as initially loaded, has a well characterized dielectric constant. Upon impact of the piston on the test bed, a shock wave is propagated through the bed in advance of the piston, with a velocity almost an order of magnitude faster than that of the piston. Shock wave propagation causes compaction of the porous media, creating a discontinuous jump in dielectric constant across the front. The reflected signal from the dielectric discontinuity at the shock (compaction) front can be accurately analyzed to give the velocity of compaction front propagation (Equation (4-3)). Calculation of the piston velocity from the reflected signal requires the use of Equation (4-5) to account for the compacted porous bed between the piston and the shock front.

The first microwave interferometric test of this apparatus used a steel tube loaded with melamine which was impacted by an aluminum piston. The microwave signal was transmitted through the inert bed of melamine, reflected off the advancing piston, back through the melamine, and out to the interferometric circuit. Superimposed on this signal was the higher frequency, lower amplitude reflection from the shock wave traveling through the melamine at a higher speed than the piston that impacted the bed. The raw data for this test are provided in Figure 4-2. An x-t plot using the simple analysis of Equation (4-4) is shown in Figure 5-15. Independent records were taken of both the piston displacement, using a streak camera, and the shock wave position, using self-shorting pressure pins mounted flush with the ID of the steel tube. The microwave data yielded a compaction front velocity of 0.61 mm/μs from the interference fringes and

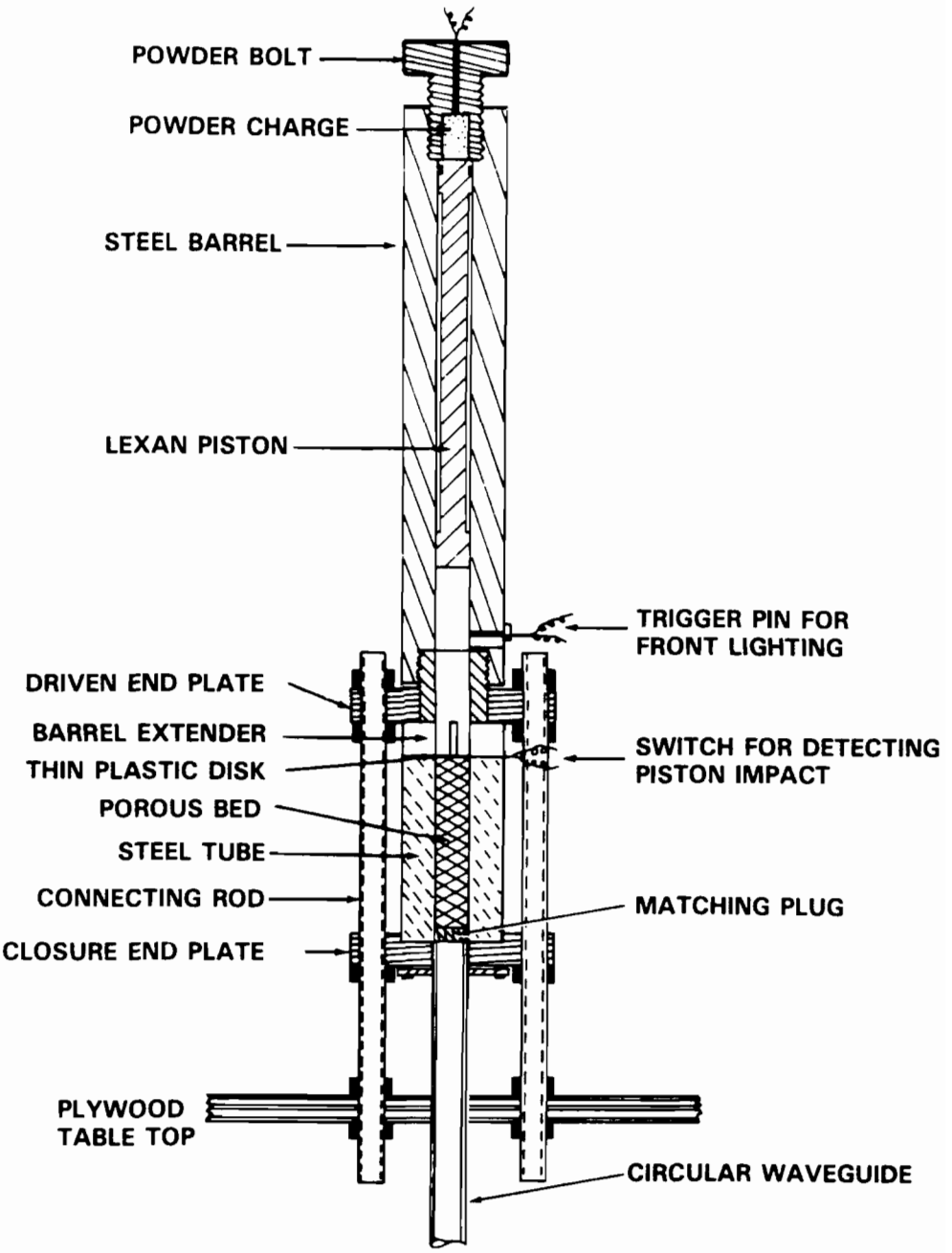

FIGURE 5-14. PDC APPARATUS INTERFACED WITH MICROWAVE INTERFEROMETER

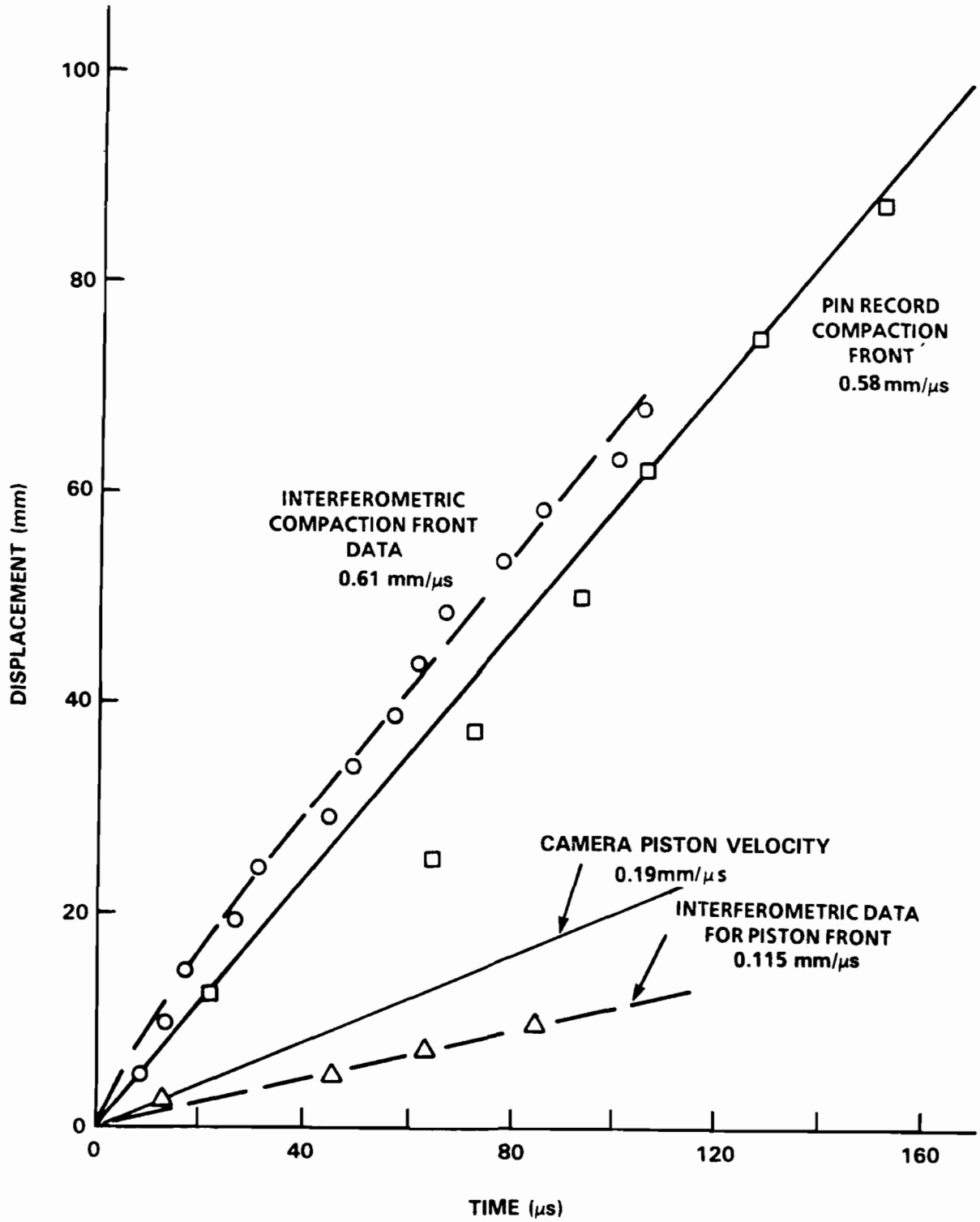

FIGURE 5-15. INITIAL REDUCTION OF SUPERIMPOSED DATA SHOWING DISAGREEMENT OF PISTON FRONT MOTION

0.58 mm/μs from the pin record (In the initial analysis where no account was made for the change in dielectric constant in the compacted region of the test bed, the piston velocity derived from the microwave signal was nearly 2 times greater than that measured by the streak camera). Investigations into the most appropriate method to incorporate the variation of dielectric constant within the compacted region into our analysis scheme were completed[16] as discussed earlier. Revised analysis results are in agreement (shown in Figure 5-16) between the microwave data and the camera data.

Further testing with this apparatus on both high explosives and propellants is reported elsewhere.[19,20,21]

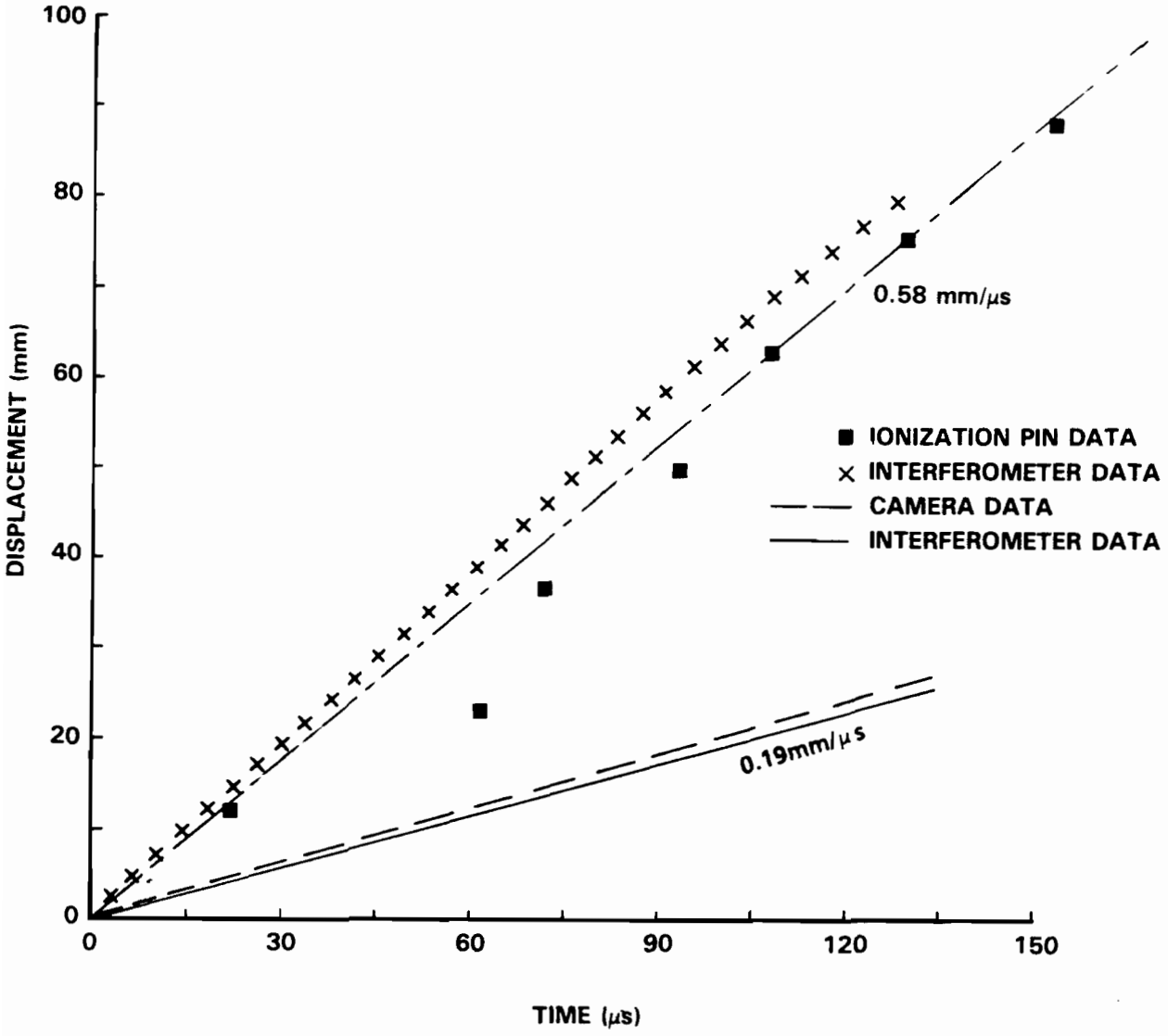

FIGURE 5-16. REVISED REDUCTION OF SUPERIMPOSED FRINGES USING EQUATION (4-5) SHOWING BETTER AGREEMENT

CHAPTER 6

COMPUTER ANALYSIS TECHNIQUES

Waveform Synthesis

Efforts to synthesize examples of the resulting waveforms as obtained from PDC testing began with sine wave synthesis. With synthesis, two separate computer generated sine waves of different magnitude, frequency, and phase were added together to give a rough estimation of the experimental data, which in turn gave insight into a more complete understanding of the reflective processes producing the output data. It was seen that the addition of harmonic reflections to pure sine waves distorted the wave shape in a manner that displayed similar charateristics to fringes recorded during experiments. The harmonics included in the synthesis were made up of second and third harmonics, each harmonic set to only a fraction of the power of the previous reflected wave amplitude. Relative phase between the waves was also treated as a variable. This displayed the most accurate representation of actual data, with the least complexity. All harmonics beyond the third were determined to be insignificant.

Fast Fourier Transform Analysis

Data analysis of past experiments has been aided by computer synthesis of expected waveforms but the final results were still being manually processed. Use of a Fast Fourier Transform (FFT) in our signal processing has subsequently been investigated. Raw output data is in the form of a discrete amplitude-time record which, when transformed into the frequency domain, defines the magnitude of the harmonics associated with the desired Doppler fundamental. A Discrete Fourier Transform (DFT) program has been adapted for use on local computers. Also, a filtering program was adapted that applies a filter to frequency domain data. It allows selective filtering of the data for removal of a range of frequencies. Either the harmonics can be removed or a single

harmonic can be selected with all else removed. The time domain data can then be viewed after filtering to assure that nothing has gone wrong.

To this point the harmonics had only been considered a detriment to accurate signal analysis. With Fourier transforms and digital filtering techniques, it was decided to attempt an analysis using the harmonics to attain higher resolution. An experiment was run to test the possibility of increasing the resolving power of the microwave interferometer by using higher order Doppler harmonics for analysis of experimental wave motion. The ability to do this is dependent on the amount of power available in the higher harmonics of the recorded data and on the resolving power of the Fourier transform analysis method to separate the harmonics from the noise. If it is possible to use the higher harmonics, it will then be possible to perform microwave measurements at centimeter wavelengths and obtain the resolution presently expected from millimeter and sub-millimeter wavelength experiments.

Raw microwave data output is obtained in the form of Doppler frequencies given by

$$2v_i = nf_{Di} * \lambda_{gi} \qquad (6\text{-}1)$$

where

n = the order of the Doppler harmonic

f_{Di} = Doppler frequency of the ith reflection

v_i = velocity of the ith reflection

λ_{gi} = guide wavelength within the media in which the i^{th} reflection moves.

Depending on the experiment, the Doppler output might be a simple sine wave of constant frequency or any combination of multiple varying frequencies and their harmonics. From the Doppler formula, v_i, the velocity of the moving reflectors, is a property of the energetic material under investigation. It is the unknown quantity to be measured and not a variable that can be changed at will. The microwave wavelength, λ_{gi}, can be changed by the experimenter, but only to a limited extent. A critical diameter required for steady state detonations in energetic materials limits the minimum usable diameter. This in turn limits the maximum microwave frequency allowed before the onset of higher

order microwave modes. Data from multiple mode experiments is too complicated to decipher using present techniques and, therefore, λ_{gi} is also limited by the material being investigated. All of this leads to the fact that f_{Di}, the Doppler output frequency, is fixed to its upper limit by the energetic material.

The number of cycles of the Doppler fringe output available to determine its frequency can then only be reasonably expanded by making the test sample longer in physical length. At least a quarter wave of the Doppler fringe output (between the point of inflection and zero slope) is required to resolve the Doppler frequency; these characteristics are usually masked from precise determination due to the addition of distortions. Fourier transformation of the output data from the time domain to the frequency domain allows the separation of harmonics from the fundamental. The nature of the resolution of the Fourier transform is such that the determination of the Doppler frequency again depends on the number of cycles available for transformation. In an effort to circumvent these apparent restrictions, it is possible to utilize one of the higher harmonics for analysis instead of the fundamental. The use of the second Doppler harmonic results in the same precision that occurs by increasing the microwave excitation frequency from 9 GHz to 18 GHz, yet avoids the higher order modes of the critical diameter problems. To test this idea analytically, the generator of the harmonics was modeled to determine which harmonics are most useful. Obviously, the higher the harmonic, the better the resolution.

The following analysis is illustrated in Figure 6-1. If a unit power is incident on a fixed boundary/interface of a lossless dielectric and if (1-p) is the fraction of the power reflected from there, then p is the power transmitted through the lossless dielectric. It is assumed that the dielectric is terminated by a perfect moving reflector, so that p is reflected with a Doppler shift and is returned to the initial boundary. At the boundary, p^2 is transmitted toward the detector, and p(1-p) is re-reflected toward the moving reflector. Here it undergoes a second Doppler shift and is then returned to the fixed boundary. Multiple reflections continue producing multiple harmonics, though each succeeding harmonic diminishes the available power. The general term for the Doppler harmonic returned to the detector in the lossless case is

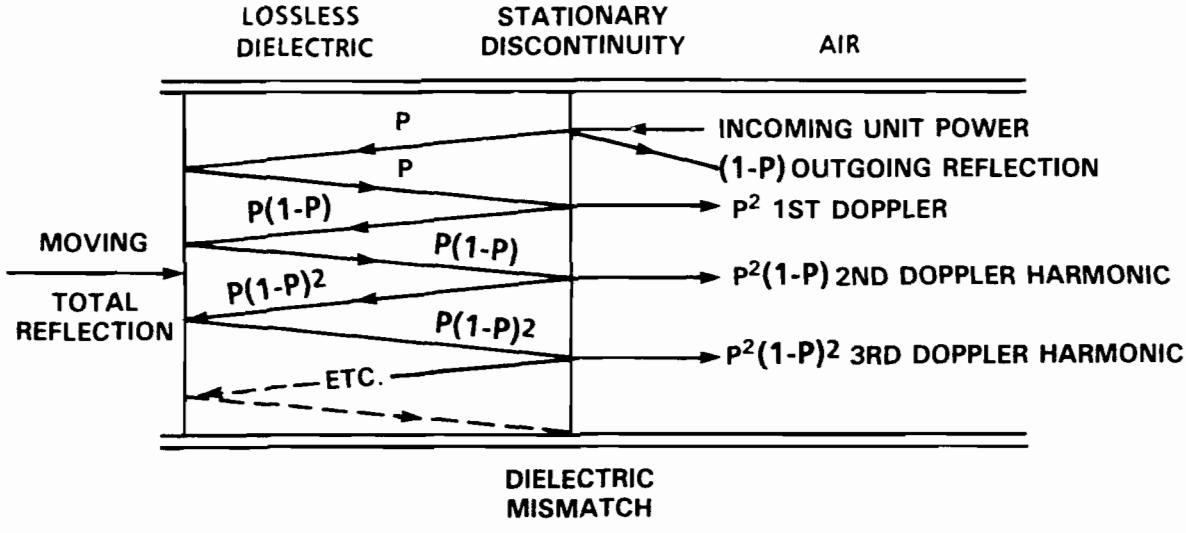

FIGURE 6-1. ANALYTICAL MODEL FOR HIGHER HARMONICS

$$p^2 * A_n(1-p)^{n-1} \qquad (6-2)$$

where n is the order of the Doppler harmonic.

To maximize the power return of any particular harmonic, the dielectric mismatch can be adjusted. Table 6-1 gives the values of the transmission coefficient needed to produce the maximum power at any given Doppler harmonic.

TABLE 6-1. VALUE OF TRANSMISSION COEFFICIENT NEEDED TO MAXIMIZE ANY PARTICULAR DOPPLER HARMONIC

Doppler harmonic A_n	Transmission Coefficient p
1	2/2 = 1 (no mismatch)
2	2/3
3	2/4 = 1/2
4	2/5
n	2/(n+1)

Given the values of Table 6-1, it is now possible to translate this information to values of dielectric constant which will produce the required reflections. It is only necessary to know the specific experimental apparatus to calculate the required value. The current reflectometer uses 25.4 mm ID circular waveguide, operated in the dominant transverse electric field mode (TE_{11}). Figure 6-2 is a plot of the required dielectric necessary to maximize a particular harmonic return. Figure 6-2 shows that the required dielectric constants are far greater than are normally encountered in energetic materials, especially if anything greater than the second harmonic is maximized. It does indicate that some gain can be obtained by lowering the operating

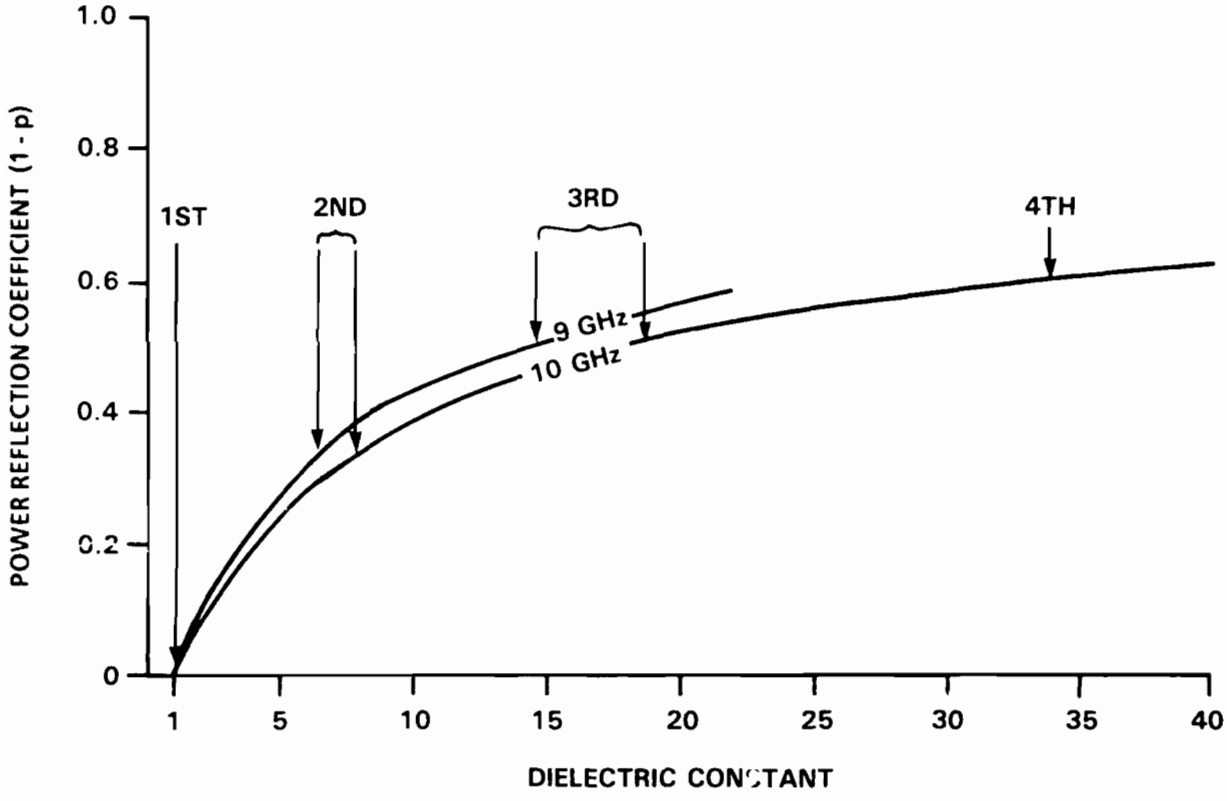

FIGURE 6-2. DIELECTRICS REQUIRED TO MAXIMIZE PARTICULAR HARMONICS

frequency and use the harmonic data. Fortunately, any dielectric discontinuity will produce some power reflection, though not a maximum, at higher harmonics. Since real experiments contain lossy materials and sometimes partially reflecting multiple fronts, it seemed more reasonable to forego the theory temporarily and perform an experiment to determine how high a harmonic is usable in the analysis of moving reflection fronts.

It was decided to repeat a previously run test (initial PDC/melamine test). Since it includes a reflecting piston driving a shock wave through an inert melamine bed, this experiment would allow a double reflection. One reflection would be from the shock wave and the other from the piston, without the added complication of a reaction of an energetic material. The major difference between this and previous experiments is that all past experiments had been carefully matched to avoid producing interface reflections. This experiment was a repeat of the previous test, but with a purposefully mismatched air to melamine interface. Also, the bed was extended in length to 305 mm (12 in) from 152 mm (6 in) to allow a longer time base for resolving the data with the Fourier transform analysis method.

Figure 6-3 depicts the amplitude-time output of this experiment. The data show a large amplitude distorted sine wave at a frequency near 5.5 kHz and a superimposed ripple about 8 times higher. The large amplitude reflection is due to the Doppler shift from the impacting piston, and the ripple is associated with reflection from the induced shock wave. If the peak-to-peak time values are scaled from the piston beats of the time domain data in Figure 6-3, there is an increase in period due to the slowing of the reflecting piston over the duration of the experiment. However, the amount of distortion present makes it very difficult to accurately deduce information from this time signal. Figure 6-4 shows the Fourier transform of the time data and shows that the lowest frequency group is centered around 5.5 kHz as a result of the piston movement. The width of this data group is a function of any change in the velocity of the piston during the experiment and how long the time base (how many cycles) existed for the piston. If the piston traveled at constant velocity for a long time with a large number of beat cycles captured, a narrow frequency spike would be expected. The second and third harmonic of the piston have been labeled on the figure. Surprisingly, no definite band of frequencies can be associated with the compaction front. The compaction front is known to exist near 40.5 kHz, noting the time of 20 cycles in Figure 6-3 and inverting the time of an average cycle.

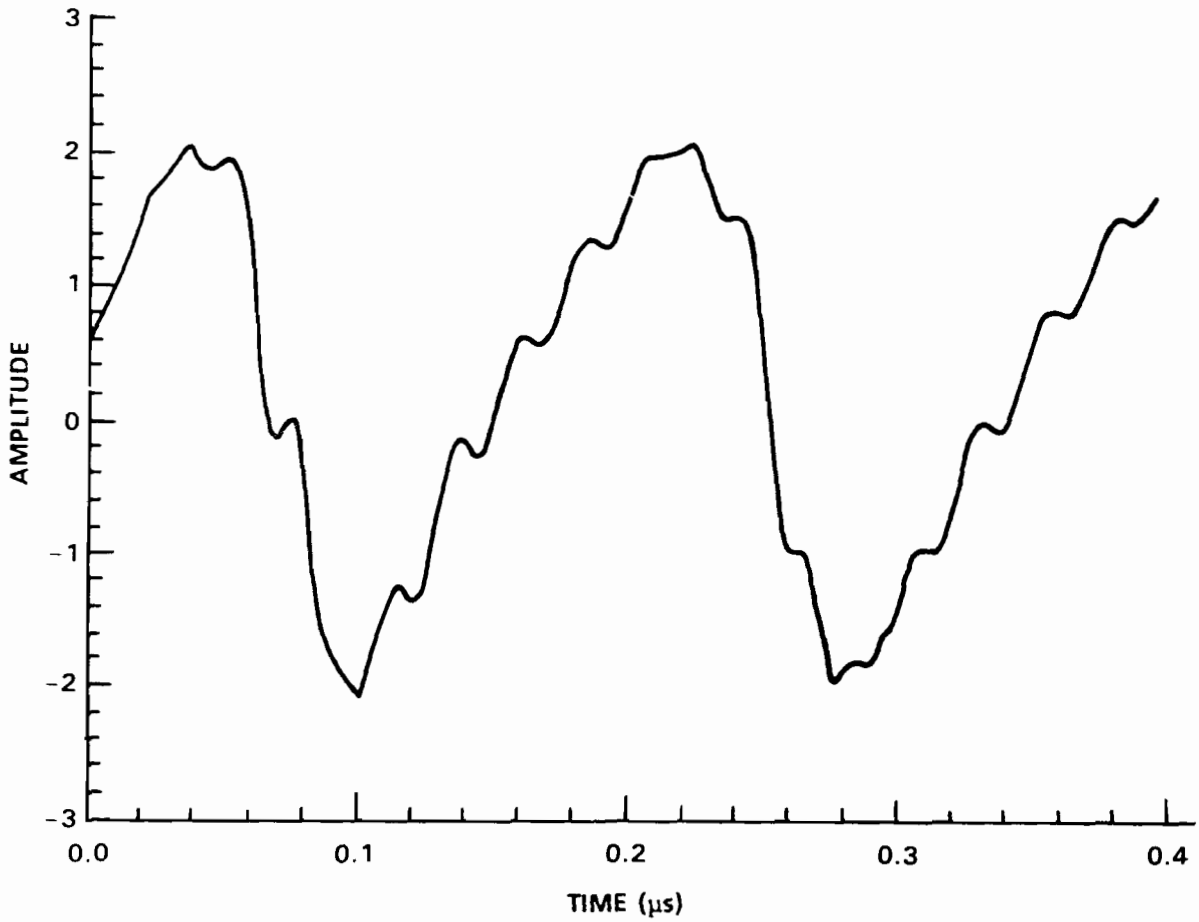

FIGURE 6-3. MELAMINE RAW DATA FRINGES WITH MISMATCHED INTERFACE

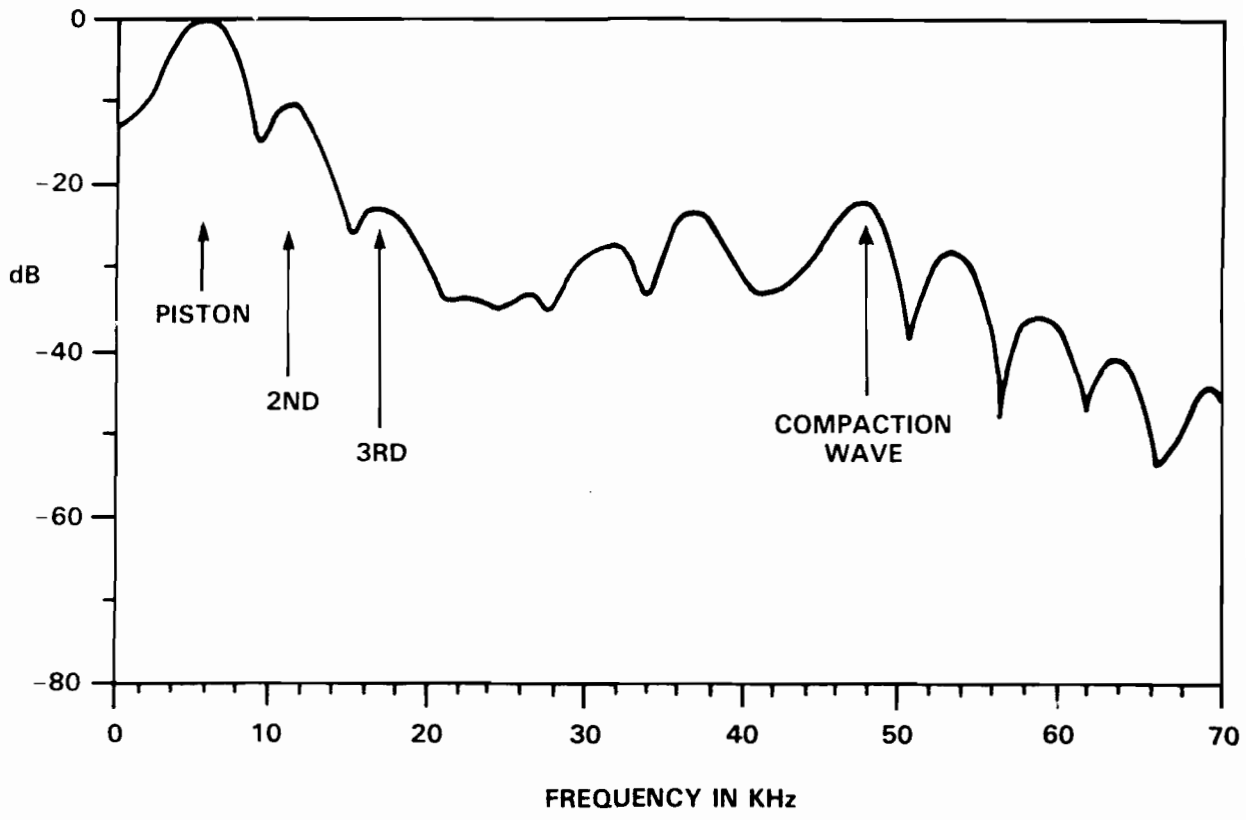

FIGURE 6-4. FREQUENCY DOMAIN DATA FROM MISMATCHED MELAMINE TEST

The object of this experiment was to attempt to determine if more precise information could be obtained by using harmonics of these fundamental reflection fronts and, to that end, the second harmonic of the piston was selected for analysis. A bandpass filter (Hanning 8.3 to 12.5 kHz) was applied in the frequency domain, then transformed back to the time domain (Figure 6-5). It is much easier here to obtain precise time values than it was with the fundamental because the filter removed the distortion. More importantly, for an equal time base, these data provide twice the information of the fundamental. Therefore, it has been demonstrated that harmonics do indeed produce a higher resolution. What remains is to find how high the most usable harmonic might be, and then the maximum resolution of the interferometer will be determined for this analysis scheme.

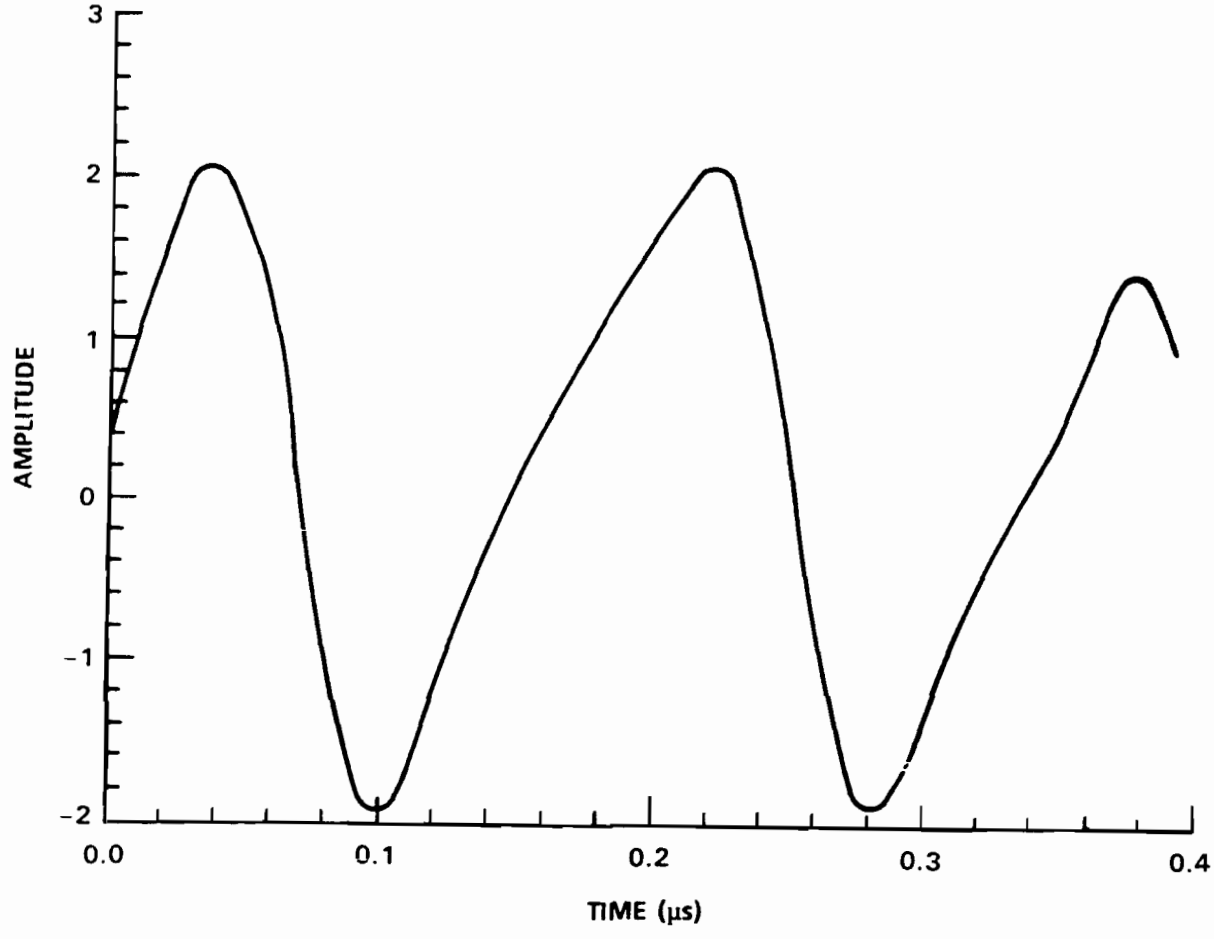

FIGURE 6-5. MISMATCHED MELAMINE DATA FILTERED TO REVEAL THE FUNDAMENTAL PISTON REFLECTION

CHAPTER 7

CONCLUSIONS AND SUMMARY

It has been demonstrated that microwave interferometry can provide information about events that occur before and after energetic materials start to release their energy. It is a non-intrusive and continuous monitoring process which can result in nearly continuous output data resolution. The output data possess information from partial reflections, which allow multiple, simultaneous processes to be viewed. With its careful application and the aid of modern signal processing techniques, microwave testing has been adapted to several energetic materials tests and analyses. In some cases, such as high confinement vessels with heavy steel walls, microwaves are the only viable source of continuous information. Microwave interferometry is not a simple technique available to the casual experiment but, as is the case of most techniques, the method requires dedicated equipment and operators.

The results from using microwave interferometry to measure the velocity of impactors, shock fronts, or reactions fronts have been shown to be comparable to conventional techniques. Two new techniques were investigated that show promise in the area of data processing. The use of Doppler harmonics and the use of Fourier transforms have demonstrated a greater resolution of reduced information in a given experiment. Determination of the dielectric constant and the requirement for accurate values have been discussed. Two methods to obtain the dielectric constant are given. It can be concluded that microwave interferometry is a useful tool for investigating reaction phenomena in energetic materials, yet its useful capabilities could be enhanced with further analytic development.

REFERENCES

1. Koch, B., "Reflexion de micro-ondes par des phenomenes de detonation," Compt. Rend. Acad. Sci., Paris, Vol. 236, pp. 661-663, 1953 [original: Lochte-Holtgreven, W., Koch, B., Zentrale f. Wissensch. Berichtswesen, Report No. 8109, 7 Nov 1944].

2. Cook, M., Doran, R., and Morris, G., "Measurement of Detonation Velocity by Doppler Effect at Three Centimeter Wavelength," Journal of Applied Physics, Vol. 26, 1955.

3. Cawsey, G., Farrands, J., and Thomas, S., "Observations of Detonation in Solid Explosives by Microwave Interferometry," Proceedings of Royal Society, London, Vol. 248A, 1958, pp. 499-521.

4. Johnson, E. G., "A Microwave Technique for Studying Detonation Phenomena," in Proceedings of Fourth Symposium (International) on Detonation, ARC-126, U.S. Naval Surface Ordnance Laboratory, Oct 1966, pp. 584-594.

5. Alkidas, A., Clary, A., Giles, G., and Shelton, S., Measurement of Steady State and Transient Solid Propellant Burning Rates with Microwaves, AFOSR TR 74-0458, Georgia Institute of Technology, Dec 1973.

6. Russell, L. H., Burning Velocities of a Solid Propellant Via a Microwave Technique, at Elevated Pressures and Pressurization Rates, NSWC TR 79-378, 1979.

7. Stanton, P. L., Venturini, E. L., and Dietzel R. W., "Microwave Interferometer Techniques for Detonation Study," in Proceedings of Eighth Symposium (International) on Detonation, NSWC MP 86-194, 1986, pp. 485-493.

8. Price D., Critical Parameters for Detonation Propagation and Initiation of Solid Explosives, NSWC TR 80-339, 1981.

REFERENCES (Cont.)

9. Ramo, S., Whinnery, J., and Van Duzer, T., Fields and Waves in Communication Electronics, Second Edition, John Wiley and Sons Inc., New York, NY, 1984

10. Glancy, B. C., and Krall, A. D., Automated Microwave Dielectric Constant Measurement System, NSWC TR 86-46, 1986.

11. Moreno T., Microwave Transmission Design Data, Sperry Gyroscope Company, 1944.

12. Dobratz B. M., LLNL Explosives Handbook, UCRL-52997, Section 10, NTIS, Springfield, VA, 1981.

13. Glancy, B. C., Krall, A. D., Invention Disclosure, Navy Case No. 70,755, 1987.

14. Lichtenecker K. and Rother K., "Logarithmisches Mischungsgesetz," Phys Z., Vol. 32, 1931, pp. 255.

15. Von Hipple, A., Dielectric Materials and Applications, LC 54-11021, 1954, John Wiley and Sons, New York, NY.

16. Sandusky, H. W., Private communications, 1987.

17. Sandusky, H., and Liddiard, T., Dynamic Compaction of Porous Beds, NSWC TR 83-246, 1983.

18. Anicin, B. A., Jojic B., Blagojevic D., Aszic, M., and Milosavljevic V., "Flame Plasma and the Microwave Determination of Solid Propellant Regression Rates," Combustion and Flame, Vol. 64, 1986, pp. 309.

19. Sandusky, H. W., Glancy, B. C., Campbell, R. L., Krall, A. D., Elban, W. L., and Coyne, P. J., Jr., "Compaction and Compressive Reaction Studies for a Spherical, Double-Base Ball Propellant," in Proceedings of the 25th JANNAF Combustion Meeting, CPIA Publ. 498, Vol. I, Oct 1988, pp. 83-94.

REFERENCES (Cont.)

20. Glancy, B. C., Sandusky, H. W., and Krall, A. D. "Dynamic Compaction and Compressive Reaction Studies for a Single-Base Ball Propellant," in Proceedings of 1989 JANNAF Propulsion Systems Hazards Subcommittee Meeting, CPIA Publ. 509, Vol. I, pp. 37-46.

21. Glancy, B. C., Sandusky, H. W., and Krall, A. D., "Dynamic Compaction and Compressive Reaction Studies for Single and Double-Base Ball Propellants," in Proceedings of the Ninth Symposium (International) on Detonation, preprints Vol. III, pp. 889-898.

DISTRIBUTION

	Copies
Commander	
Naval Air Systems Command	
Attn: Library	1
AIR-932H	1
AIR-932T	1
AIR-932F (B. Sobers)	1
Department of the Navy	
Washington, DC 20361	
Commander	
Naval Sea Systems Command	
Attn: SEA-99612	1
SEA-62D	1
SEA-62D31	1
SEA-06G42	1
Department of the Navy	
Washington, DC 20362	
Director	
Strategic Systems Programs	
Attn:SP2731(J. Culver)	1
SP273 (E. Throckmorton)	1
Department of the Navy	
Washington, DC 20376	
Commanding Officer	
Naval Propellant Plant	
Attn: Technical Library	1
Indian Head, MD 20640	
Director	
Defense Advanced Research Projects Agency	1
Washington, DC 20301	

	Copies
Office of Naval Technology	
Attn: ONT-21 (E. Zimet)	1
ONT-213 (D. Siegel)	1
ONT-23 (A. Faulstich)	1
ONT-232 (D. Houser)	1
Department of the Navy	
800 North Quincy Street	
Arlington, VA 22217	
Commander	
Naval Weapons Center	
Attn: Technical Library	1
Code 326B (L. Josephson)	1
Code 3266 (D. Lind)	1
Code 326B (G. Greene)	1
Code 3891 (M. Chan)	1
Code 3858 (R. Yee)	1
Code 3264 (H. Gollmar)	1
Code 385 (R. Atkins)	1
Code 3265 (J. Pakulak)	1
Code 38 (R. Derr)	1
Code 389 (T. Boggs)	1
Code 3891 (C. Price)	1
Code 3891 (A. Atwood)	1
Code 3891 (H. Richter)	1
China Lake, CA 93555	
Commanding Officer	
Naval Research Laboratory	
Attn: Technical Information Section	2
4555 Overlook Ave., S.W.	
Washington, DC 20375	

DISTRIBUTION (Cont.)

	Copies
Commanding Officer Naval Weapons Station Attn: R & D Division	1
Code 50, NEDED	1
Code 505, NEDED	1
Yorktown, VA 23691	
Air Force Office of Scientific Research Attn: Library Bolling Air Force Base Washington, DC 20332	1
Department of the Air Force AFAL/MKPL, Stop 24 Attn: C. Merrill Edwards AFB, CA 93523-5000	1
Georgia Institute of Tech. Attn: Prof. E. Price School of Aerospace Eng. Atlanta, GA 91125	1
Superintendent Naval Academy Attn: Library Annapolis, MD 21402	1
Lockheed Missiles-Space Co. Attn: Naval Plant Representative Office, SPL-332	1
P. Noble (Org. 83-10, Bldg. 157-3W)	1
P.O. Box 504 Sunnyvale, CA 94086	
Commanding Officer Naval Ordnance Station Louisville, KY 40124	1
Hercules Incorporated Allegany Ballistics Laboratory Attn: Library P. O. Box 210 Cumberland, MD 21502	1
Joint Venture of Hercules and Thiokol Attn: A. Butcher P.O. Box 98 Magna, UT 84044	1
Redstone Scientific Information Center U. S. Army Missile Command Attn: Chief, Documents Redstone Arsenal, AL 35809	1
Commanding Officer Army Armament Research and Development Command Energetic Materials Division Attn: DRSMC-LCE (N. Slagg)	1
DRSMC-LCE (J. Alster)	1
Dover, NJ 07801	
Commanding Officer Harry Diamond Laboratories Attn: Library 2800 Powder Mill Road Adelphi, MD 20783	1
Army Ballistic Research Laboratories Attn: SLCBR-IB-I (D. Kooker)	1
SLCBR-BL-EE (R. Frey)	1
Aberdeen Proving Ground Aberdeen, MD 21005-5066	

DISTRIBUTION (Cont.)

	Copies
Armament Development & Test Center	
Attn: DLOSL/Technical Library	1
AFATL/MNE (G. Parsons)	1
AFATL/MNE (T. Floyd)	1
AFATL/MNW (D. Wagnon)	1
Eglin Air Force Base, FL 32542	
United Technologies Chemical Systems	
Attn: R. Hermsen	1
Building 50121	
P.O. Box 50015	
San Jose, CA 94515-0015	
Director	
Applied Physics Laboratory	
Attn: Library	1
Johns Hopkins Road	
Laurel, MD 20707	
Thiokol/Huntsville Division	
Attn: Technical Library	1
Huntsville, AL 35807	
Research Director	
Pittsburgh Mining and Safety Research Center	
U. S. Bureau of Mines	
4800 Forbes Avenue	
Pittsburgh, PA 15213	1
Defense Technical Information Center	
Cameron Station	
Alexandria, VA 22304-6145	12

	Copies
Goddard Space Flight Center	
NASA	
Glenn Dale Road	
Greenbelt, MD 20771	1
Lawrence Livermore National Laboratory	
University of California	
Attn: Library	1
D. Aldis	1
L. Green	1
E. James	1
E. Lee	1
P. Urtiew	1
A. Weston	1
P. O. Box 808	
Livermore, CA 94550	
Sandia National Laboratories	
Attn: M. Baer	1
J. Cummings	1
J. Nunziato	1
P. Stanton	1
G. Venturini	1
P. O. Box 5800	
Albuquerque, NM 87115	
Superintendent	
Naval Postgraduate School	
Attn: Library	1
Monterey, CA 93940	
Chairman	
DOD Explosives Safety Board	
Attn: J. Ward	1
2461 Eisenhower Avenue	
Alexandria, VA 22331	

DISTRIBUTION (Cont.)

	Copies
Director Los Alamos National Laboratory Attn: Library	1
A. Bowman	2
J. J. Dick	1
B. Dobratz	1
J. McAfee	1
B. Asay	1
J. Ramsay	1
L. Stretz	1
P. O. Box 1663 Los Alamos, NM 87544	
Aerojet Ordnance and Manufacturing Co. 9236 East Hall Road Downey, CA 90241	1
CETR New Mexico Tech. Attn: P. Anders Persson	1
Socorro, NM 87801	
Zernow Technical Service Center Attn: Dr. L. Zernow	1
425 W. Bonita Ave., Suite 208 San Dimas, CA 91773	
Commanding Officer Naval Underwater Systems Center Attn: LA 151 (Technical Library)	1
Newport, RI 02840	
Library of Congress Attn Gift & Exchange Div.	4
Washington, DC 20540	
Loyola College Attn: Prof. W. Elban	1
Prof. P. Coyne	1
Department of Engineering Science 4501 N. Charles Street Baltimore, MD 21210	
Advanced Technology and Research, Inc. Attn: A. D. Krall	1
14900 Sweitzer Lane Laurel, MD 20707	

DISTRIBUTION (Cont.)

	Copies
Internal Distribution:	
E231	2
E232	3
E35 (GIDEP Office)	1
R	1
R04	1
R10	1
R101	1
R10A	1
R10B	1
R10C	1
R10D	1
R10E	1
R10F	1
R11	1
R12	1
R12 (P. Spahn)	1
R13	1
R13 (R. Bardo)	1
R13 (S. Coffey)	1
R13 (D. Demske)	1
R13 (J. Forbes)	1
R13 (B. Glancy)	10
R13 (P. Gustavson)	1
R13 (S. Jacobs)	1
R13 (R. Lee)	1
R13 (E. Lemar)	1
R13 (D. Price)	1
R13 (H. Sandusky)	2
R13 (G. Sutherland)	1
R13 (D. Tasker)	1
R13 (W. Wilson)	1
R14	1
R15	1
R16	1
R30	1
R31	1
R40	1
R42	1
R43	1